FABRICATION AND CHARACTERIZATION OF SUPERCONDUCTOR YBCO JOSEPHSON JUNCTIONS

A Thesis Submitted to
the Graduate School of Engineering and Sciences of
İzmir Institute of Technology
in Partial Fulfillment of the Requirements for the Degree of

MASTER OF SCIENCE

in Physics

by
Berrin Pınar ALGÜL

February 2008
İZMİR

We approve the thesis of **Berrin Pınar ALGÜL**

Prof. Dr. Doğan ABUKAY
Supervisor

Prof. Dr. Mustafa GÜDEN
Committee Member

Assoc. Prof. Dr. Lütfi ÖZYÜZER
Committee Member

29 February 2008
Date

Assoc. Prof. Dr. Lütfi ÖZYÜZER
Head of Physics Department

Prof. Dr. Hasan BÖKE
Dean of the Graduate School of
Engineering and Science

ACKNOWLEDGMENTS

It is my pleasure to express my sincere gratitude to my supervisor Prof. Dr. Doğan Abukay for his support throughout this study.

I am thankful to Prof. Dr. Mustafa Tepe for his support as well as his understanding in letting us use the laboratories at Ege University.

I have been lucky to have had the chance to meet and work with Dr. Ilbeyi Avci. I am deeply indebted to him for instructing me in the appropriate attitudes towards research as well as his guidance, support and encouragement.

I would like to express my sincere thanks to Dr. Rizwan Akram for sharing his experience and friendship.

I am thankful to my friends in the Physics Departments at Izmir Institute of Technology and Ege University for their friendship.

Finally, I would like to express my gratitude and love to my family who has always supported and encouraged me.

ABSTRACT

FABRICATION AND CHARACTERIZATION OF SUPERCONDUCTOR YBCO JOSEPHSON JUNCTIONS

A well-controlled, high-yield Josephson junction production process forms the basis of superconducting electronic device and circuit technology. In order to use the Josephson junctions effectively and fabricate them reproducibly, their structural and electrical characterization should be performed.

This study concentrates on the fabrication and characterization of high temperature bicrystal grain boundary Josephson junctions fabricated onto 24-dand 30-degree $SrTiO_3$ bicrystal substrates using high quality $YBa_2Cu_3O_{7-\delta}$ (YBCO) thin-films.

200 nm thick YBCO thin films were deposited using a dc Inverted Cylindrical Magnetron Sputtering technique by investigating the thin film deposition conditions in order to obtain device quality films. The superconducting properties of the thin films were determined by electrical characterizations, consisting of resistance versus temperature and magnetic susceptibility versus temperature measurements. Structural properties were analyzed by Atomic Force Microscope, Scanning Electron Microscope and X-Ray Diffraction.

Prepared thin film samples were patterned as bicrystal grain boundary Josephson junctions by standard photolithography and chemical etching processes. The current-voltage characteristics of the Josephson junctions were performed at 77 K under zero and non-zero applied field in magnetically shielded environment. The critical current values (I_c), normal resistance (R_n) and I_cR_n product of the output signals were determined, and the values were discussed as function of the film growth conditions. The optimization of the Josephson junctions was performed in order to improve both the signal performance and the stability of our devices against thermal cycling.

ÖZET

SÜPERİLETKEN YBCO JOSEPHSON EKLEMLERİ YAPIMI VE KARAKTERİZASYONU

Üstün performanslı, kararlı ve kontrol edilebilen Josephson eklemleri süperiletken elektroniği aygıtlarının temelini oluşturur. Üretimi tekrarlanabilir Josephson eklemleri için uygun bir üretim teknolojisinin geliştirilmesi ve verimli bir şekilde çalıştırılabilmesi için, aygıtların yapısal ve elektriksel karakterizasyonlarının ayrıntılı olarak yapılması gerekmektedir.

Bu çalışmada, 24 ve 30 derecelik yönelime sahip çift kristal alttaşlar üzerinde YBCO ince filmlerle grain boundary Josephson eklemlerinin üretimi ve karakterizasyonu amaçlanmıştır.

Bu çalışmada kullanılan Josephson eklemleri için 200 nm kalınlığında YBCO ince filmler kullanılmış ve bu filmler magnetron püskürtme yöntemi kullanılarak üretilmiştir. İnce film üretim koşullarının aygıt performansı üzerindeki etkisinin öneminden yola çıkılarak, ince film kalitesinin arttırılması için üretim koşullarında iyileştirme çalışmaları yapılmıştır. Üretilen ince filmlerin özellikleri, direnç-sıcaklık ve manyetik süseptibilite-sıcaklık ölçümleriyle belirlenmiş, yapısal özellikleri ise Atomik Kuvvet Mikroskobu, Taramalı Elektron Mikroskobu ve X-Işını Kırınımı analizleriyle incelenmiştir.

İnce filmlere Josephson eklemi formu verilmesi amacıyla fotolitografik desenleme ve kimyasal aşındırma işlemleri uygulanmıştır. Üretilen Josephson eklemleri daha sonra aygıt performanslarına bağlı olarak karakterize edilmiştir. Eklemler kritik akım (I_c), normal durum direnci (R_n) ve I_cR_n çarpımlarına göre karakterize edilmiş ve bu değerler ince film üretim koşullarında değişlikler yapılarak iyileştirilmeye çalışılmıştır. Eklemlerin akım-gerilim karakterizasyonları sıfır ve sıfırdan farklı manyetik alanlar altında sıvı azot sıcaklığında (77 K) yapılmıştır. Aygıtların termal çevrimlere karşı dayanıklılığını ve performanslarını artırmak amacıyla eklem optimizasyonu çalışmaları yapılmıştır.

TABLE OF CONTENTS

LIST OF FIGURES viii

LIST OF TABLES xi

CHAPTER 1. INTRODUCTION 1

CHAPTER 2. JOSEPHSON EFFECT 4

2.1. General Description of Josephson Effect 4

2.2. The DC Josephson Effect 5

2.3. The AC Josephson Effect 6

2.4. Feynman Derivation 7

2.5. Dynamics of Josephson Junctions 10

2.5.1. Junction in Magnetic Field 10

2.5.2. Current-Phase Relation 12

2.5.3. Current-Voltage Characteristics 12

CHAPTER 3. JOSEPHSON JUNCTIONS: TYPES AND MODELS 17

3.1. Tunnel Junction and Weak Links 17

3.2. High Temperature Josephson Junctions 19

3.3. Grain Boundary Josephson Junctions 20

3.3.1. Bicrystal Grain Boundary Interfaces 22

3.4. The Properties of YBCO 22

CHAPTER 4. EXPERIMENTAL TECHNIQUES 25

4.1. Device Fabrication 25

4.1.1. Junction Mask Design 2

4.1.2. Substrate Preparation and Cleaning 26

4.1.3. Film Deposition by dc magnetron sputtering 28

4.1.4. Photolithographic Process 29

4.1.5. Etching 33
4.1.6. Contact Metallization (Gold Deposition) 35
4.2. Measurement Setup 36
4.3. Characterization Techniques 38
4.3.1. Surface Characterization 38
4.3.1.1. AFM 39
4.3.1.2. SEM 39
4.3.2. XRD 40
4.3.3. Electrical Characterization 40
4.3.3.1. AC Magnetic Susceptibility Measurement 40
4.3.3.2. Resistance-Temperature Measurements 41
4.3.3.3. Current-Voltage Measurements 43
4.3.3.4. Critical Current vs. Magnetic Field Measurement 44

CHAPTER 5. RESULTS AND DISCUSSION 45
5.1. Resistance vs. Temperature Measurements 45
5.2. Magnetic Susceptibility-Temperature Measurements 48
5.3. Structural Analyses 49
5.4. Current-Voltage Characteristics 52
5.4.1. I-V Characteristics in the Absence of Magnetic Field 53
5.4.2. Width dependence of Josephson Critical Current 56
5.4.3. Magnetic Field Dependence of Josephson Critical Current 57
5.5. Optimization Process of Josephson Junctions 58
5.5.1. Deposition Rate Dependence of Josephson Junctions 58
5.5.2. Effects of Thermal Cycles on I-V Characteristics of JJs 63

CHAPTER 6. CONCLUSION 66

REFERENCES 68

LIST OF FIGURES

Figure **Page**

Figure 2.1. The model of potential of the insulator V(x) and the magnitude of the wavefunction $|\psi|$ 7

Figure 2.2. $I_c(\phi)$ for a single short Josephson junction when the self-fields have been neglected. 11

Figure 2.3. Equivalent circuit for Josephson junction. Parallel combination of basic Josephson junction, capacitor *C* and constant resistor *R*. 14

Figure 2.4. Nonhysteretic I-V characteristic of overdamped Junctions $(\beta_c << 1)$. Here β_c values can be chosen from 0 to 1. 15

Figure 2.5. Hysteretic I-V characteristic of underdamped junctions $(\beta_c >> 1)$. Here β_c values exceed 1. 16

Figure 3.1. Different type JJs. 19

Figure 3.2. Grain boundary Josephson junction types. a) Step-Edge SNS Junction, b) Ramp-Edge Junction, c) Step-Edge GB Junctions, d) Bicrystal GB Junction 21

Figure 3.3. Crystal structure of YBCO orthorhombic phase 23

Figure 4.1. Josephson junctions mask layouts 26

Figure 4.2. YBCO thin film deposition process. 29

Figure 4.3. Pictures of home made spinner used for photoresist coating 30

Figure 4.4. Picture of hot plate used for soft and hard baking 31

Figure 4.5. The pictures of OAI mask aligner having automatic controlled compact UV source, and patterned, Josephson junctions. 32

Figure 4.6. Photolithography process. a) YBCO thin film deposited on top of the STO substrate, b) Spin-coating of photoresist on top of the YBCO thin film, c) Chrome mask placement and alignment on top of the photoresist, d) UV exposure to photoresist through the chrome mask, e) Developing the

photoresist, f) Etching of the YBCO film after lithography and subsequently removing the resist from the film surface. 34
Figure 4.7. Sputter coater used for gold contacts 35
Figure 4.8. Wire bonder used for contacts 36
Figure 4.9. BNC box and junction probe designed to measure the junctions 37
Figure 4.10. Electrical measurement setup used for obtaining current-voltage characteristics of the junctions and μ-metal shield implemented into the cryogenic dewar.. 38
Figure 4.11. Labview program for χ-T and R-T measurements.. 41
Figure 4.12. Labview program for I-V measurements. 43
Figure 4.13. Magnetic field dependence measurement setup 44
Figure 5.1. Optical microscope image of YBCO thin film. 46
Figure 5.2. R-T graph of 24 degree bicrystal substrate across the grain boundary line and two sides of the line. 46
Figure 5.3. R-T curves of YBCO thin films across the grain boundary lines of 24- and 30-degree STO bicrystal substrates. 47
Figure 5.4. Temperature dependence of magnetic susceptibility of different samples.. 48
Figure 5.5. XRD peaks of YBCO Thin Films. 49
Figure 5.6. (a) Roughness analyses of the junction strip line 50
Figure 5.6. (b) Junction profile 50
Figure 5.6. (c) Edge profile of the junction. 51
Figure 5.7. (a) SEM image of the junction pattern 51
Figure 5.7. (b) SEM image of closer view of the junctions 52
Figure 5.7. (c) SEM image of grain boundary line of the 24^0 bicrystal STO substrate. 52
Figure 5.8. (a) I-V characteristic of junctions on 24-degree bicrystal STO substrate.. 54
Figure 5.8. (b) I-V characteristic of junction on 30-degree bicrystal STO substrate.. 55

Figure 5.9. Junction width dependence of the I-V curves on a) 20-degree, b) 30-degree bicrystal STO substrate..... 56
Figure 5.10. Magnetic field dependence of Josephson junction with 4μm width on 24-degree bicrystal substrate.. 57
Figure 5.11. R-T curves of YBCO thin films deposited at different deposition rates relatively 1.2, 1.6 and 2.0 nm/min.. 58
Figure 5.12. . AFM images of YBCO thin films along the grain boundary region of bicrystal substrate depending on the film deposition rates of a) 1.2 nm/min, b) 1.6 nm/min, c) 2 nm/min..... 59
Figure 5.13. X-ray diffraction spectra of YBCO films grown at different deposition rates. 60
Figure 5.14. I-V characteristics of the GB Josephson junctions deposited at different rates. 62
Figure 5.15. (a) I-V characteristic of JJs at 77 K depending on the thermal cycles. Unprotected JJ, Solid, dotted and dashed lines represent the measurements for the first, 15^{th} and 30^{th} thermal..... 64
Figure 5.15. (b) JJ with amorphous YBCO layer. Solid, dotted and dashed lines represent the measurements for the first, 15^{th} and 30^{th} thermal cycles respectively. 66

LIST OF TABLES

Table **Page**

Table 4.1. The unit cell spacing for YBCO and $SrTiO_3$ 27

Table 4.2. Resistance-temperature values of the Pt-111. 42

Table 5.1. The deposition parameters, transition temperatures, FWHM values and surface roughness of three different YBCO thin films with the same thickness of 200 nm. 61

Table 5.2. Properties of three different Josephson junctions as function of the YBCO thin film deposition rate. 62

CHAPTER 1

INTRODUCTION

Josephson effect and Josephson junctions are the underlying principle and technology behind most superconducting electronic devices(Gross, et al. 1997, Weinstock, et al. 1993, Delin, et al. 1995). There has recently been tremendous progress in the development of devices based on high-temperature superconducting Josephson junctions fabricated from $YBa_2Cu_3O_{7-\delta}$ (YBCO) thin films such as the Superconducting Quantum Interference Device (SQUID). In addition, Josephson junctions provide active elements for ultra fast low-power digital electronics (Likharev, et al. 1991, Beha 1982, Tahara, et al. 2001). They are also candidate for the technology of future quantum computers (Anocker 1980). As in the conventional silicon-based (semiconductor) electronics, further miniaturization is a key research issue in superconducting electronics.

A Josephson junction is composed of two superconductors separated by a thin insulating barrier. Cooper pairs can tunnel or diffuse through the barrier, forming a current with no voltage appearing across the junction (Josephson 1962, Anderson and Rowel 1963). Josephson junctions and devices utilizing them have been fabricated using conventional low-temperature superconductors, usually using an SIS (superconductor/insulator/superconductor) configuration. In contrast to low-temperature superconducting junctions, many junction structures have been investigated for high-temperature superconductors in order to fabricate reproducible and controllable junctions (Pagone and Barone 1997). Since the first report on the fabrication of a natural grain-boundary Josephson junction using YBCO, there have been many efforts in the fabrication of Josephson junctions and SQUIDs based on different device constructions. Bicrystal grain boundary, biepitaxial grain boundary, step-edge grain boundary, step-edge superconductor/normal-metal/superconductor (SNS), ramp-edge SNS, locally damaged superconducting line by ion beams and interface-engineered junctions are the most commonly investigated configurations (Koelle, et al. 1999).

Small-scale device applications require thin film form of superconductors in both low-T_c and high-T_c materials. The discovery of superconductivity in ceramic

oxides (Bednorz and Muller 1986) such as $YBa_2Cu_3O_{7-\delta}$ (YBCO) (Wu, et al. 1987) with transition temperature (T_c) above boiling point of liquid nitrogen (77 K) generated a worldwide enthusiasm in research towards development of new superconducting technologies for both large- and small-scale applications. The recent progress on superconducting electronics device application is driven by the expectation that superconductors cooled in liquid nitrogen at 77 K would be more widely used than superconductors cooled in liquid helium (^{4}He) at 4.2 K. There are two major reasons behind this expectation: liquid nitrogen is much cheaper than liquid helium and, for a given heat load, liquid nitrogen boils away much more slowly than liquid helium.

In order to develop widely used superconducting electronic device technology, one looks for a process that yields highly reproducible parameters for building Josephson junctions. It is also essential, especially for low-T_c applications, to develop an appropriate interconnect technology, which is a multi-level process that enables one to fabricate two intersecting superconducting films separated by a thin insulating layer and superconducting contacts through the insulating layer. The major challenge in the development of high-T_c electronics circuits in general is the need to develop an appropriate technology for Josephson junctions. There have been many approaches to develop Josephson junctions with stable parameters for both low-T_c and high-T_c devices. In low-T_c processes on niobium (Nb), the fabrication parameters have almost been standardized (Gurvitch, et al. 1983). In high-T_c processes, many approaches have been tried, including single layer YBCO to multilayer devices. It seems that single layer processing of YBCO, in which grain-boundary junctions are formed along the misorientation boundary of a bicrystal substrate or at a step-edge milled in a substrate, is the most suitable technology for developing stable junctions in high-T_c superconducting electronics. Despite the recent progress in the high-T_c SQUID systems and applications, it seems fair to say that an ideal technology has not been invented (Koelle, et al. 1999).

In high-T_c superconducting electronics, among wide variety of compounds, YBCO has been mostly used as superconducting thin film because of its appropriate crystalline structure to ensure both high critical current densities in the *ab* plane and relatively acceptable low levels of *1/f* noise (Haage, et al. 1997). Among the current candidates for thin film superconducting materials, only YBCO can supply sufficiently strong flux pinning at *77 K* by its c-axis normal to the substrate (c-axis films). In addition, the growth mechanism of YBCO has been well understood to achieve high

quality thin films on a number of substrates by *in situ* processes with a variety of deposition techniques (Avci, et al. 2004, Liu, et al. 2002)

Josephson junctions, especially high-T_c Josephson junctions, are the strong candidates for future electronics applications, but their production parameters are still not well defined as discussed above. Therefore, they should be discussed in detail in order to understand the physical phenomena lying behind and to achieve a successful fabrication technique that yields high performance Josephson junctions (JJs) on YBCO thin films.

This thesis is organized in three main parts. Theoretical background and different types of Josephson junctions are discussed in Chapter 2 and Chapter 3. The experimental methods involving fabrication of high temperature Josephson junctions and measurement techniques at liquid nitrogen temperature are explained in Chapter 4. The main results on studied devices are presented in Chapter 5. The thesis is summarized in Chapter 6.

CHAPTER 2

JOSEPHSON EFFECT

2.1. General Description of Josephson Effect

Josephson Effect is a direct manifestation of the macroscopic quantum coherence of superconducting state. In 1962, Brian D. Josephson, then a graduate student at Cambridge University made a remarkable prediction that the case of two superconductors weakly coupled by a thin insulating barrier that allows quantum mechanical tunneling of Cooper pairs without breaking up the pairs from one side to other side even with no potential difference (Josephson 1962). Before 1962 the general consensus related with Cooper pairs tunneling through a thin insulating layer was that such an event would not happen enough to be measurable. The reason was that as the tunneling of an electron has a very small change of occurring, the tunneling of electrons in a Cooper pair simultaneously crossing the insulator would be astronomically small. However Brian Josephson changed this common belief. From his calculations using BCS theory he discovered that probability of Cooper pair tunneling through the barrier was the same as that for a single electron. The reason is that the tunneling for a Cooper pair is an ordered, coherent process. In other words we should not imagine the situation to be two electrons' waves leaking across the insulating layer. Instead, it is the macroscopic wavefunction that tunnels from one superconductor to the other (Orlando and Delin 1990).

The Josephson Effect is observed, if two superconductors are weakly connected by electrical contacts. In the following such a contact will be denoted as Josephson junctions. The Cooper pairs on each side of the junction can be represented by a single wavefunction. In fact all the Cooper pairs in a superconductor can be described by a single macroscopic wavefunction which is 2π periodic because phase is single valued (Golubov, et al. 2004). The wavefunctions for cooper pairs on the electrodes of the junction penetrate into the insulating region and lock together in phase. They are said to be phase coherent. Under these conditions, a current (supercurrent) will flow through the junction in the absence of an applied voltage up to a maximum critical value. However there is a limit to the amount of current that Cooper pairs can carry and so if

too much current is applied, the Josephson effect is lost and the current is carried by normal electrons. I_C (the Josephson critical current) is known as the maximum dc current can be carried through the junction by Cooper pair $I_S = I_C . \sin \Delta\varphi$ where $\Delta\varphi$ difference in phase across the junction.

His further prediction is that if a finite DC voltage is applied across the junction which is enough to break Cooper pairs, normal electrons will tunnel and carry current. However the applied current is less than enough to break up Cooper pairs a voltage increases the energy of Cooper pairs respond by oscillating back and forth across the junction. So $\Delta\varphi$ evolves according to $\frac{d(\Delta\varphi)}{dt} = \frac{2eV}{\hbar}$ so that the current which can be carried through the junction as an alternating current of amplitude I_C with frequency $w = \frac{2eV}{\hbar}$.

In 1963, these effects were observed experimentally shortly afterwards by Anderson (Anderson and Rowell 1963) and then active research efforts were started in order to understand and study the physical structure of Josephson Effect. These prediction and observation led to the award of the 1973 Nobel Prize to Josephson and Anderson. Josephson's discovery has contributed not only the science of superconductivity but also to quantum mechanics.

2.2. The DC Josephson Effect

All the electrodynamics phenomena taking place at the Josephson junctions are generally divided into stationary (dc) and non-stationary (ac) effects depending on whether the variables, including the phase difference φ, change with time or not. In the dc Josephson effect phase φ remains constant, voltage across the junction is zero and Josephson current density is always smaller than the critical current density.

$$\text{V=0},\ \varphi(t) = \text{constant},\ \ I = I_s(\varphi),\ \ |I| \le I_c \qquad (2.1)$$

A sufficiently small current can pass through a Josephson junction without dissipation. In other words when such a current passes through the junction, no voltage is generated across the junction. Since the current is always small, the magnetic field generated itself can be neglected. An important characteristic of the junction is the phase gradient. The phase difference across the junction is,

$$\varphi = \varphi_2 - \varphi_1 \tag{2.2}$$

where φ_1 and φ_2 are the phases of wavefunctions in the first and second superconducting electrodes. Now one needs to find to the relation between current through the junction, I_S, and phase difference φ.

$$I_s = I_c \sin(\varphi) \tag{2.3}$$

2.3. The AC Josephson Effect

The ac Josephson effect occurs when the phase changes with time. So far we have considered the case of $I \langle I_C$ through the junction. If the current supplied by an external source exceeds the critical value I_C, it causes a voltage V appears across the junction. The behavior of a quantum-mechanical system is described by the Schrödinger equation as

$$i\hbar \frac{\partial \psi}{\partial t} = H\psi \tag{2.4}$$

where, H is the Hamiltonian of the system. The wavefunctions of a stationary state ψ_1 satisfies the equation

$$H\psi_1 = E\psi_1 \tag{2.5}$$

where, E is the energy of the state $\psi_1 = \psi_1 . e^{i\theta(t)}$, with $|\psi_1|$ being independent of time. On substitution into (Equation 2.5) we get

$$-\hbar \frac{\partial \theta}{\partial t} = E \tag{2.6}$$

The presence of the voltage V across the junction suggests that the Cooper pair energies in superconductors on either side of the junction, E_1 and E_2, are related to each other by

$$E_1 - E_2 = 2eV \tag{2.7}$$

because the charge of pairs 2e. Substituting (Equation 2.7) to (Equation 2.6) we obtain the second fundamental Josephson equation

$$2eV = \hbar \frac{\partial \varphi}{\partial t} \tag{2.8}$$

2.4. Feynman Derivation

It is possible to follow several different approaches in order to obtain basic Josephson relations. An elegant phenomenological derivation of the Josephson relations which was based on a "two level system" picture was given by Feynman (Feynman, et al. 1965). This approach despite its simplicity, offers a powerful key for the understanding of the peculiar features of Josephson Phenomena.

Let us consider the tunneling structure of superconductor-barrier-superconductor. We call ψ_1 and ψ_2 the pair wave function for the right and left superconductors. As discussed earlier, we are dealing with macroscopic quantum states. Therefore, each superconducting electrode can be described by a single quantum state and the ψ's can be regarded as macroscopic wave functions, so that $|\psi|^2$ represents the actual Cooper pair density *n*. In this simple symmetrical case, the material on both sides is assumed to be the same under zero magnetic field. The two amplitudes can then be related in the following way:

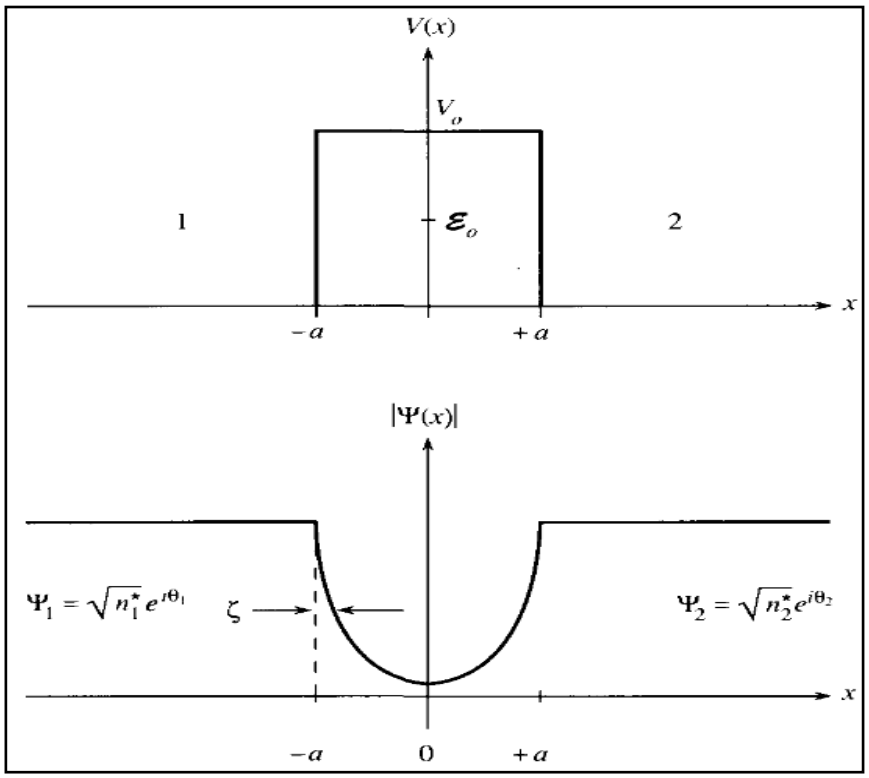

Figure 2.1. The model of potential of the insulator V(x) and the magnitude of the wavefunction $|\psi|$ (Source: Orlando 1991)

The two superconductors have densities of superconducting electron pairs n_1^* and n_2^* respectively.

ψ_1 is the common wave function of all electrodes on one side, and ψ_2 is the corresponding function on the other side. Let us take the junction as symmetric under zero magnetic field for simplicity

$$\frac{\delta\psi_1}{\delta t} = -\frac{i}{\hbar} E_1 \psi_1 \tag{2.9.a}$$

$$\frac{\delta\psi_2}{\delta t} = -\frac{i}{\hbar} E_2 \psi_2 \tag{2.9.b}$$

If we consider existing of weak coupling between two superconductors, transition occurs between two states. This coupling is essentially related to the finite overlap of the two pair wavefunctions ψ_1 and ψ_2. This situation can be taken into account that an additional coupling is introducing into the (Equation 2.9)

$$\frac{\delta\psi_1}{\delta t} = -\frac{i}{\hbar} E_1 \psi_1 + K\psi_2 \tag{2.10.a}$$

$$\frac{\delta\psi_2}{\delta t} = -\frac{i}{\hbar} E_2 \psi + K\psi_1 \tag{2.10.b}$$

In our case, the coupling means that cooper pairs can be exchanged between superconductor 1 and superconductor 2. The coupling strength is symmetric and fixed by the coupling constant K. ψ_1 and ψ_2 describe macroscopic states occupied by a large number of particles. Then, we can interpret the square of the amplitude in terms of the particle density n_s of the Cooper pairs. So we can write:

$$\psi_1 = \sqrt{n_{s1}} e^{i\varphi_1} \tag{2.11.a}$$

$$\psi_2 = \sqrt{n_{s2}} e^{i\varphi_2} \tag{2.11.b}$$

Taking derivatives of the wave functions:

$$\frac{\partial\psi_1}{\partial t} = \frac{\dot{n}_{s1}}{2\sqrt{n_{s1}}} e^{i\varphi_1} + i\sqrt{n_{s1}} e^{i\varphi_1} \tag{2.12.a}$$

$$\frac{\partial\psi_2}{\partial t} = \frac{\dot{n}_{s2}}{2\sqrt{n_{s2}}} e^{i\varphi_2} + i\sqrt{n_{s2}} e^{i\varphi_2} \tag{2.12.b}$$

$$\frac{\dot{n}_{s1}}{2\sqrt{n_{s1}}}e^{i\varphi_1}+i\sqrt{n_{s1}}e^{i\varphi_1}+i\sqrt{n_{s1}}e^{i\varphi_1}\dot{\psi}_1=-\frac{i}{\hbar}(E_1\sqrt{n_{s1}}e^{i\varphi 1}+K\sqrt{n_{s2}}e^{i\varphi_2}) \tag{2.13.a}$$

$$\frac{\dot{n}_{s2}}{2\sqrt{n_{s2}}}e^{i\varphi_2}+i\sqrt{n_{s2}}e^{i\varphi_2}+i\sqrt{n_{s2}}e^{i\varphi_2}\dot{\psi}_2=-\frac{i}{\hbar}(E_2\sqrt{n_{s2}}e^{i\varphi_2}+K\sqrt{n_{s1}}e^{i\varphi_1}) \tag{2.13.b}$$

by separating imaginary and real parts,

$$\frac{1}{2}\frac{\dot{n}_{s1}}{\sqrt{n_{s1}}}=\frac{K}{\hbar}\sqrt{n_{s2}}\sin(\varphi_2-\varphi_1) \tag{2.14.a}$$

$$\frac{1}{2}\frac{\dot{n}_{s2}}{\sqrt{n_{s2}}}=\frac{K}{\hbar}\sqrt{n_{s1}}\sin(\varphi_1-\varphi_2) \tag{2.14.b}$$

$$i\sqrt{n_{s1}}\dot{\psi}_1=-\frac{i}{\hbar}(E_1\sqrt{n_{s1}}+K\sqrt{n_{s2}}\cos(\varphi_2-\varphi_1) \tag{2.15.a}$$

$$i\sqrt{n_{s2}}\dot{\psi}_2=-\frac{i}{\hbar}(E_2\sqrt{n_{s2}}+K\sqrt{n_{s1}}\cos(\varphi_1-\varphi_2) \tag{2.15.b}$$

Because of the exchange of Cooper pairs between 1 and 2,

$$\dot{n}_{s1}=-\dot{n}_{s2}\ \text{(Change of particle density)} \tag{2.16}$$

$$\dot{n}_{s1}=\frac{2K}{\hbar}n_{s1}\sin(\varphi_2-\varphi_1)=-\dot{n}_{s2} \tag{2.17}$$

Temporal change of particle density multiplied by the volume yields the change of the particle number and hence the particle current across the junction becomes

$$I_s=I_c\sin(\varphi_2-\varphi_1) \tag{2. 18}$$

This is the dc Josephson relation. A supercurrent can flow through the junction up to a maximum value of I_c. For currents larger than I_c, a potential difference is developed across the junction. The difference between the phases of the wave functions of the superconductors is

$$\varphi=\varphi_2-\varphi_1 \tag{2.19}$$

The term $\cos(\varphi)$ in (Equation 2.15) can be eliminated by subtraction to give:

$$\frac{\partial\varphi}{\partial t}=\frac{2e}{\hbar}v \tag{2.20}$$

This is the ac Josephson relation. Integration of (Equation 2.20) and substitution into (Equation 2.18) gives

$$I_s = I_c \sin\left(\frac{2e}{\hbar}Vt + \varphi_0\right) \tag{2.21}$$

where φ_0 is a constant of the integration. The phase difference between the order parameters of the two superconductors increases linearly with time.

Therefore, when the junction is voltage biased, ac current-flow at an angular frequency ω is given by

$$\omega = \frac{2e}{\hbar}v \tag{2.22}$$

The Josephson junction, therefore, acts as a natural voltage tunable microwave oscillator. A dc voltage of 1mV across the junction produces a frequency of 483.6 GHz.

2.5. Dynamics of Josephson Junctions

2.5.1. Josephson Junction in Magnetic Field

One of the defining facts of a superconductor is that it screens magnetic fields; an applied field will only penetrates a very short distance, known as the *London penetration depth* λ**,** into the superconductor before it decays completely. The size of λ varies for different superconductors. In Josephson junctions there is a similar effect; the Josephson currents will screen the magnetic fields formed inside the junction (Rowell 1963). The field will penetrate a distance λ_j known as the *Josephson penetration depth*

$$\lambda j = \sqrt{\frac{\phi_0}{2\pi J_c(2\lambda + d)}} \tag{2.23}$$

where *d* is the thickness of the insulating barrier, J_c is the critical current density and ϕ_0 is the magnetic flux quantum which is a constant defined as *h/2e* and equal to 2 x10^{-15} *Wb*. Since λ_j depends on J_c it can vary with orders of magnitude even the junctions made of same material; λ_j is very important since it determines the "magnetic size" of the junction. If the junction width *w* is bigger than λ_j, then we need to take into account its self-field and screening currents when studying how the junction parameters are affected by an external magnetic field. If a junction with *w* smaller than λ_j, the field will

penetrate uniformly into the junction, and hence the junction is considered as "short", whereas if $w > \lambda_j$, the flux dynamics of the junction starts to be important and the junction is considered as "long" (Gross and Marx 2005). Unless a junction is very narrow, its dynamics will be affected by even relatively moderate fields. This is true even for magnetically short junctions. In other words, in a junction with certain width, the properties change as we move along the interface in the presence of a distributed field-gradient (Kadin 1999). In a conventional rectangular junction with uniform current distribution, it is straightforward to describe the effect of the external field. It turns out the critical current through the junction, which has a familiar dependence on the external flux ϕ,

$$I_c(\phi) = I_c \left| \frac{\sin(\frac{\pi\phi}{\phi_0})}{\frac{\pi\phi}{\phi_0}} \right| \tag{2.24}$$

This is nothing else but the well known Fraunhofer diffraction pattern as can be seen in Figure 2.2. This pattern is identical to what one finds if a beam of light passes through a narrow rectangular slit.

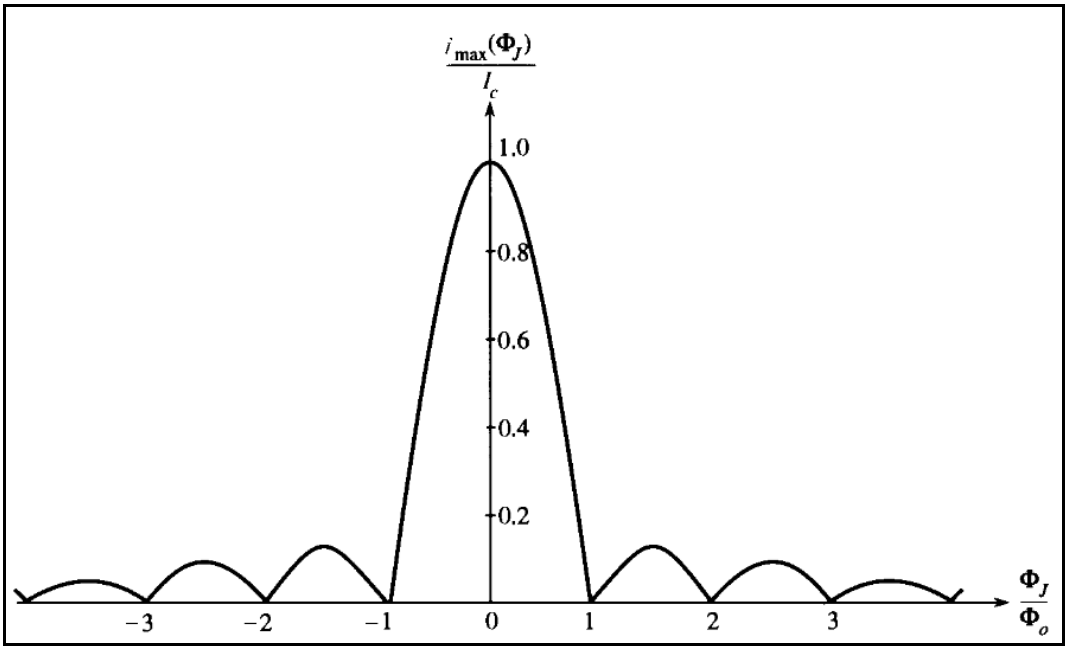

Figure 2.2. $I_c(\phi)$ for a single short Josephson junction when the self-fields have been neglected (Source: Anderson and Rowell 1964)

2.5.2. Current-Phase Relation

There are several properties of the Current-Phase relation that are rather general and depend neither on the junctions' materials and geometry nor on the theoretical model used to describe the process in the junction (Golubov, et al. 2004). These are:

- Changing the phase across the junction by 2π should not change the physical state of the junction. Hence, the change must not influence the supercurrent $I_s(\phi)$ across the junction and the current-phase relation (CPR) is a 2π-periodic function

$$I_s(\varphi) = I_s(\varphi + 2\pi) \tag{2.25}$$

- Changing the direction of the supercurrent flow across the junction must cause a change in the sign of the phase difference, therefore;

$$I_s(\varphi) = -I_s(-\varphi) \tag{2.26}$$

- A dc supercurrent can flow only if there is a phase gradient of the order-parameter. Hence, in the absence of phase difference, $\phi=0$, there should be zero supercurrent

$$Is(2\pi) = 0 \qquad n=0, \pm 1, \pm 2, ... \tag{2.27}$$

Summarizing our discussion we can conclude that the density between two junction electrodes in the most general case should have the form

$$I_s(\varphi) = \sum_{n\geq 1} \left\{ I_n \sin(n\varphi) + J_n \cos(n\varphi) \right\} \tag{2.28}$$

Here, I_n is the critical current or maximum Josephson current, which is determined by the coupling strength between two junction electrodes. (Expression 2.28) is the general formulation of the first Josephson equation. It is also denoted as the current-phase relation, since it relates the supercurrent density to phase difference.

2.5.3. Current-Voltage Characteristics

Josephson junction and its electronic properties should be described in two cases: zero voltage state and voltage state (Barone and Paterno 1982, Gross and Marx 2005, Hadfield 2002). In zero voltage state, Josephson current density J_s is always smaller than the maximum current density J_c so that the current is flowing only as supercurrent without any additional excess current, thus residing the junction in static

state. In the voltage state, the junction current is larger than the maximum Josephson current and therefore only a part of total current can be carried by Cooper pairs. In this case, in addition to the Josephson current, the total current flowing through the junction includes other current channels carrying the excess current, thus residing the junction in a finite voltage state. These current channels are resistive channel and capacitive channel.

The resistive channel belongs to the normal electron tunneling through the junction. The origin of the normal electrons that can tunnel in the superconducting state at even zero temperature is due to the breaking up of Cooper pairs by applied voltage. If the Cooper pairs is considered as having a binding energy of twice the energy gap, then when the voltage exceeds the value of energy gap the Cooper pairs will be unbound and become normal electrons. Once the normal electrons are present in the system, they can tunnel through the barrier and cause resistance.

At non-zero temperatures, beside the superelectrons, normal electrons already exist in superconductor. At temperature above zero temperature, because of the thermal excitation, there is a probability of broken Cooper pairs generating normal electrons, thus creating resistance. The capacitive channel due to the finite capacitance of Josephson junction since it can be considered as parallel plate capacitor having a capacitance C. In the presence of time varying junction voltage there exist finite displacement current across the junction due to the capacitance (Likharev 1986).

The case of including resistive and capacitive current channels in addition to the supercurrent is known as generalized Josephson junction. The normal electron tunneling due to the resistive channel has nonlinear junction conductance $G(v)$ depending on the voltage and temperature, because the junction resistance due to the normal electron tunneling is depends on the gap voltage for the current smaller than the critical current and depends on the normal state resistance for the current grater than the junction critical current. This gives us two conditions for the junction conductance in certain ranges: gap voltage and normal state resistance. To describe the response of the junction to a dc driving source, we first have to describe a model including the constant conductance that is independent of the voltage, $G(v)=1/R$, for simplifying the current-voltage characteristics of the Josephson junction by assuming the resistance as constant and normal state resistance. This is known as the resistively shunted junction model (RSJ model) (Tinkham 1996) For the case of *RSJ model* of the junction driven by a dc source, the current expression is

$$I = I_c \sin\varphi + \frac{1}{R}\frac{\phi_0}{2\pi}\frac{d\varphi}{dt} + C\frac{\phi_0}{2\pi}\frac{d^2\varphi}{dt^2} \qquad (2.\ 29)$$

By simplifying this relation to a dimensionless equation, we have

$$\frac{I}{I_c} = \sin\varphi + \frac{d\varphi}{d\xi} + \beta_c \frac{d^2\varphi}{d\xi^2} \qquad (2.30)$$

Where $\xi = \left(2\pi I_c R/\phi_0\right)t$ and $\beta_c = 2\pi I_c R^2 C/\phi_0$ which is known as *Stewart-McCumber parameter* (Stewart 1968, McCumber 1968) and characterizes the hysteretic behavior of the current-voltage characteristics of the junction by measuring the importance of the capacitance (Tinkham 1996). The current-voltage characteristics of the Josephson junction can be analyzed in two limiting cases for describing the hysteretic behavior: overdamped and underdamped junction cases.

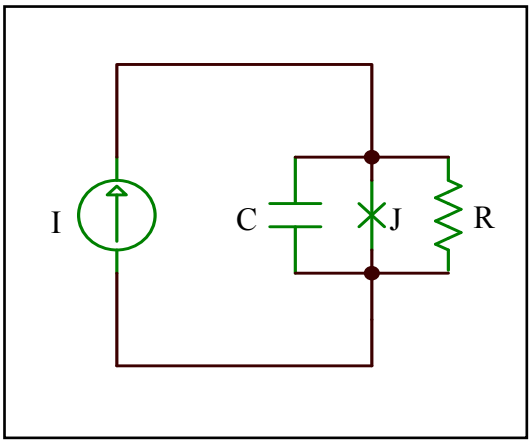

Figure 2.3. Equivalent circuit for Josephson junction. Parallel combination of basic Josephson junction, capacitor C and constant resistor R (Source: Barone and Paterno 1962)

In *overdamped* case, $\beta_c << 1$, the equivalent circuit is described as simply parallel combination of the basic Josephson junction and a constant resistor *R,* equation (2.30) reduces to

$$\frac{I}{I_c} = \sin\varphi + \frac{d\varphi}{d\xi} \qquad (2.31)$$

For $I \le I_c$, it is expected that all the current flows as supercurrent and φ does not depend on the time. Then we obtain the relation for the phase difference as

$$\varphi = \sin^{-1}\left(\frac{I}{I_c}\right) \qquad \text{For } I \le I_c \qquad (2.32)$$

This resides the junction in zero voltage state until the current reaches up to critical value. For $I \ge I_c$, the current can no longer flow as a pure supercurrent. Some of the current must then flow through the resistor creating a voltage that will cause φ to change in time. Then we can rewrite the current-phase relation as $d\xi = d\varphi/\left(I/I_c - \sin\varphi\right)$. Integration results in a periodic function $\varphi(t)$ with period $T = \dfrac{\phi_0/I_c R}{\sqrt{\left(I/I_c\right)^2 - 1}}$. Using $\left\langle V(t)\right\rangle = \dfrac{1}{T}\int_0^T V(t)dt = \dfrac{\phi_0}{T}$, this yields a time-averaged voltage as a function of current

$$\left\langle V(t)\right\rangle = I_c R\sqrt{\left(\frac{I}{I_c}\right)^2 - 1} \qquad \text{For } I \ge I_c \qquad (2.33)$$

By these relations in (2.32) and (2.33) we have a nonhysteretic I-V characteristic for the case of overdamped junctions ($\beta_c << 1$).

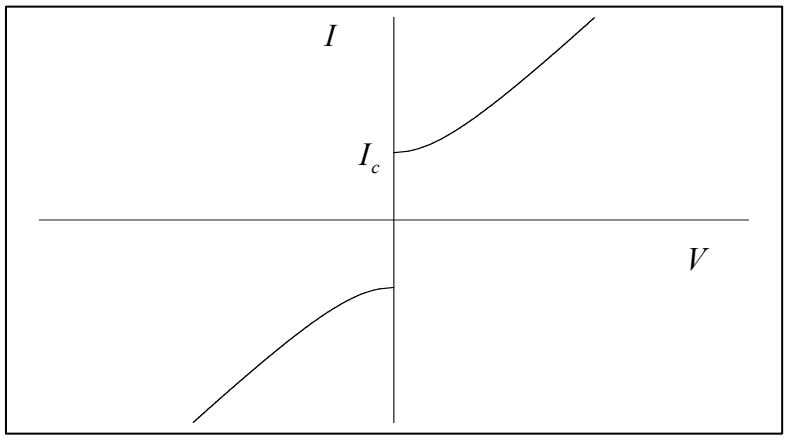

Figure 2.4. Nonhysteretic I-V characteristic of overdamped Junctions $(\beta_c << 1)$. Here β_c values can be chosen from 0 to 1 (Source: Steward and McCumber 1968)

In *underdamped* junction case, $\beta_c >> 1$, the equivalent circuit is described as junction with a parallel combination of a resistor and a capacitor having a dominant capacitive charging in the junction. In this case of underdamped junction, the current-voltage characteristic shows hysteretic behavior. For raising current, the superconducting state is maintained up to a critical current I_c. For decreasing current, the superconducting state is reached if the current is $I_{c,min,}$ lower than I_c. For β_c values exceeds 1, a hysteretic curves are obtained as following.

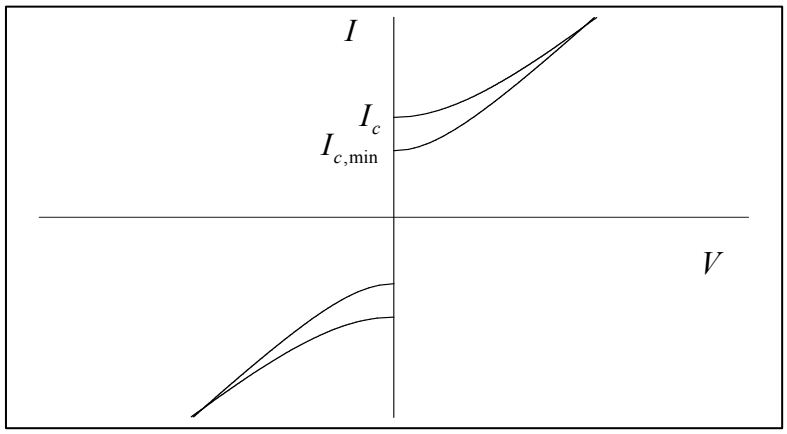

Figure 2.5. Hysteretic I-V characteristic of underdamped junctions $(\beta_c >> 1)$. Here β_c values exceed 1 (Source: Steward and McCumber 1968)

CHAPTER 3

JOSEPHSON JUNCTIONS: TYPES AND MODELS

3.1. Tunnel Junctions and Weak Links

A prominent role in research during the history of prediction and discovery of Josephson effect was played by superconducting tunnel junctions in which two superconducting electrodes are separated by a thin insulating layer. Finite conductivity is exhibited in such structures only due to tunneling electrodes thorough the potential barrier created by an insulator. A finite supercurrent may flow in them owing to the correlated tunneling of the electrons forming a pair. These are the tunnel junctions for which the Josephson effect was predicted and it main consequences were observed experimentally: the flow of supercurrent without any voltage drop and the specific magnetic field dependence of the supercurrent. The out standing role of tunnel junctions has greatly affected further research field. Some workers were led to believe that this effect could take place only in tunnel junctions, although the Josephson effect was observed in structures with non-tunnel conductivity as early 1964 (Anderson and Dayem 1964)

Initially Josephson current was observed in a junction made from two superconductors separated by a thin insulating layer, typically $10\,A^0$. However Josephson effect can be observed different types of structure according to current transport properties through the junction (Likharev 1986). These are tunnel type and non-tunnel type junctions (weak links). The latter consists of different types of weak links. The expression weak link accounts for these structure which present direct superconductivity between the superconducting electrodes through a narrow bridge of semiconducting normal metal, superconducting materials or short, narrow constrictions. These structures differ from tunnel junctions with direct conductivity (non-tunnel type) between superconducting electrodes. Figure 3.1 shows the pictures of different type JJs. Different types of weak links can e summarized as follows;

If a normal metal, usually 0.1 to 10 μm thick, is interposed as an interlayer between two superconductors, S-N-S sandwich type junction is obtained in Figure 3.1.c. A finite current can flow through such a junction due to the well known proximity effect

(De Gennes 1964). The effect lays in the fact that if a normal metal and a superconducting metal are brought into proper electrical contact, some Cooper pairs will penetrate into the normal metal from the superconductor. Thus in the normal metal there arises a nonzero order parameter Δ, which exponentially decreases within the metal over a distance of the order of "normal coherence length" or "decay length",ζ. On the other hand, the values of Δ in the superconductor over the distances of the order of coherence length from the boundary will become smaller than equilibrium value. Hence, if the thickness of the normal interlayer is not very large, the order parameter will be different from zero throughout the normal metal, and a finite supercurrent may flow through the interlayer.

As a normal interlayer we may use either a true metal which does not suffer superconducting transition at any temperature or a superconductor having a critical temperature $0<T_c<T$. Moreover, a sandwich material may also be superconducting in which case the weakness of the link is to be provided by keeping its critical current small compared to that of the electrode material *S*. In this case the junction called the *S*-*S'*-*S* sandwich.

A situation closely resembling the sandwich phenomenon can be created in proximity effect bridges or in ion implanted bridges. In both cases a section of low critical current, usually about a few microns long, is made in a narrow strip of superconducting film. In the first case this section is formed by the proximity effect with a normal metal under layer, and in the second case by the implantation of ions into this region. In practice, the only distinction between these structures and sandwiches is that their cross section can be made much smaller because one of the dimensions is formed by thin film deposition.

An entirely different method of forming weak links is realized in a constant-thickness bridge or in a variable-thickness bridge. The geometry of weak links is more complicated in the two others type of Josephson junctions in point contacts and blob-type junctions. In the first case the electrical contact is created by touching of the two superconducting electrodes, and in the second case forming a pellet of solder (superconducting at low temperatures) over a length of a superconducting wire.

Such weak links, especially point contacts, have found wide range application due to the simplicity of their fabrication. A significant disadvantage of these structures

as subject of for physical research is their poorly defined geometry. Their demerit in practical applications is their irreproducibility.

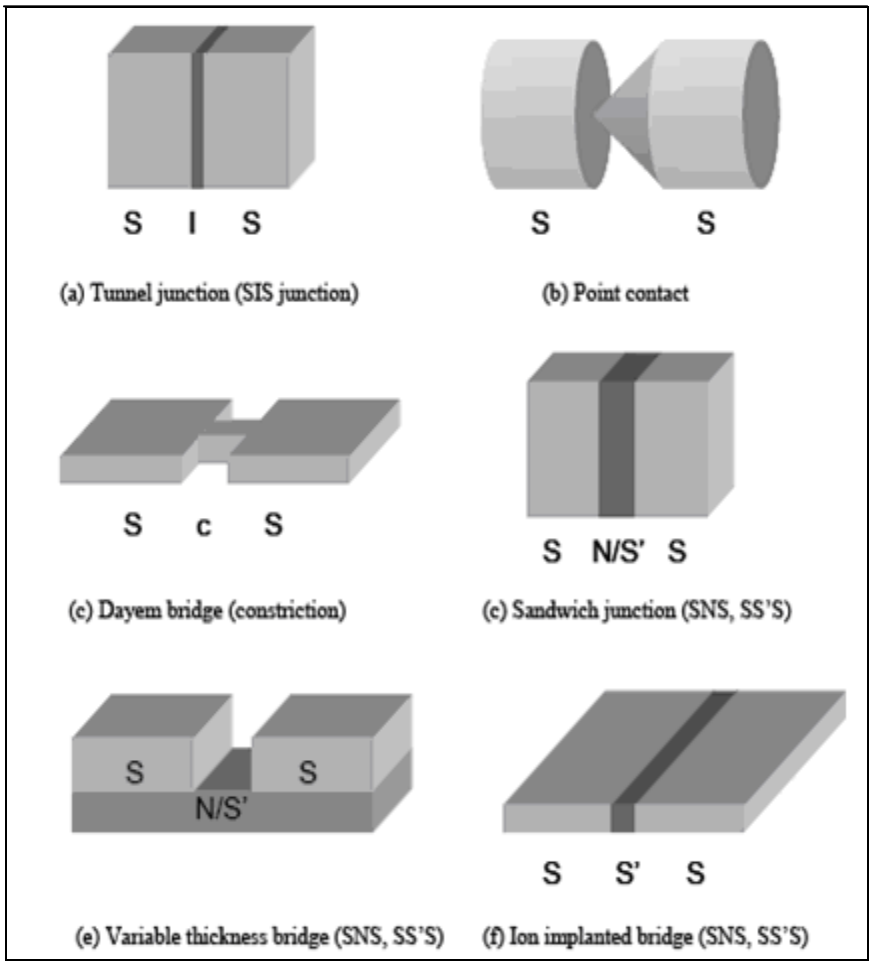

Figure 3.1. Different type of Josephson junctions
(Source: Likharev 1979)

3.2. High Temperature Josephson Junctions

There is encouraging progress in the fabrication of useful high temperature superconducting devices based on JJs (Gross, et al. 1997). However, up to date the ideal approach in HTS-JJ technology satisfying all requirements for complex integrated circuit still can not be identified (Gross 1994). For the metallic low temperature superconductors the most successfully used junction technology is based on multilayer structure. For the HTS the fabrication of such a structure is very difficult because of complex structure of high T_c oxide materials. Requirements for a successful Josephson junction technology include non-hysteretic I-V characteristics, with properties close to

the predictions of the RSJ model, a high I_cR_N product, controllable and reproducible parameters, high yield, high stability under room temperature storage and thermal cycling, and low 1/f noise (Koelle 1999). These requirements are very well established in low-T_c junctions based on *Nb*. Unfortunately, a comparable high-T_c technology does not yet exist (Wördenweber 1999, Beasley 1999). Because:

- In contrast to *Nb*, high-T_c materials require epitaxial growth imposing sever constrains on the choice of materials and processing techniques.
- Secondly, Again in contrast to *Nb*, the superconducting coherence length ζ is short and highly anisotropic, typically 2 nm in the a-b plane and 0.2 nm in the c-axis direction. As a result the properties of high-T_c materials are highly susceptible to structural and chemical changes an atomic length scales. Thus, the superconducting electrodes need to have perfect crystallinity and a well defined interface has to be achieved.
- Thirdly, the barrier materials are generally oxides close to a metal-insulator transition with a complex structure and a strong sensitivity to defects on an atomic length scale.

As a result, transport across the barrier is highly dependent on microstructural imperfections in the barrier and its interface with the electrodes. Thus, a well-defined barrier with high crystalline quality and homogeneity is required. Due to the difficulties related to the fabrication technology of HTS-JJ, the use of grain boundary Josephson junctions (GBJJs) are still favorable.

3.3. Grain Boundary Josephson Junctions

Since the fabrication method for direct-tunnel junction structure (SIS) for high-T_c superconductors has not been invented yet because of the material complexity and growth process limitation on oxide superconductors, weak-link has became a significant alternative to achieve Josephson effect in these materials (Tafuri and Kirthley 2005, Neils 2002). The term “weak-link” means the connection of two superconducting electrodes, realizing the conducting junction, in which the critical current is much less in contact region than that of electrodes, hence obtaining a weakly coupling Josephson-like behavior (Ayache 2006). The main advantage of the weak-link junctions can be considered as having smaller junction capacitance than the capacitance of the tunnel

junctions based on the coupling of two superconductors with a thin insulating barrier between them(). The most used weak-link junction type is the grain boundary junction fabricated on bicrystal substrate. With the natural properties of weak-links, the high-T_c YBCO grain boundary junctions show well defined RSJ type behavior due to their small capacitance and relatively high normal state resistance (Dimos, et al. 1990). The principle of the grain boundary junction technology, illustrated in Figure 3.2, consists of growing a film epitaxially on a bicrystalline substrate, which contains a grain boundary of the desired configuration Figure 3.2.d.

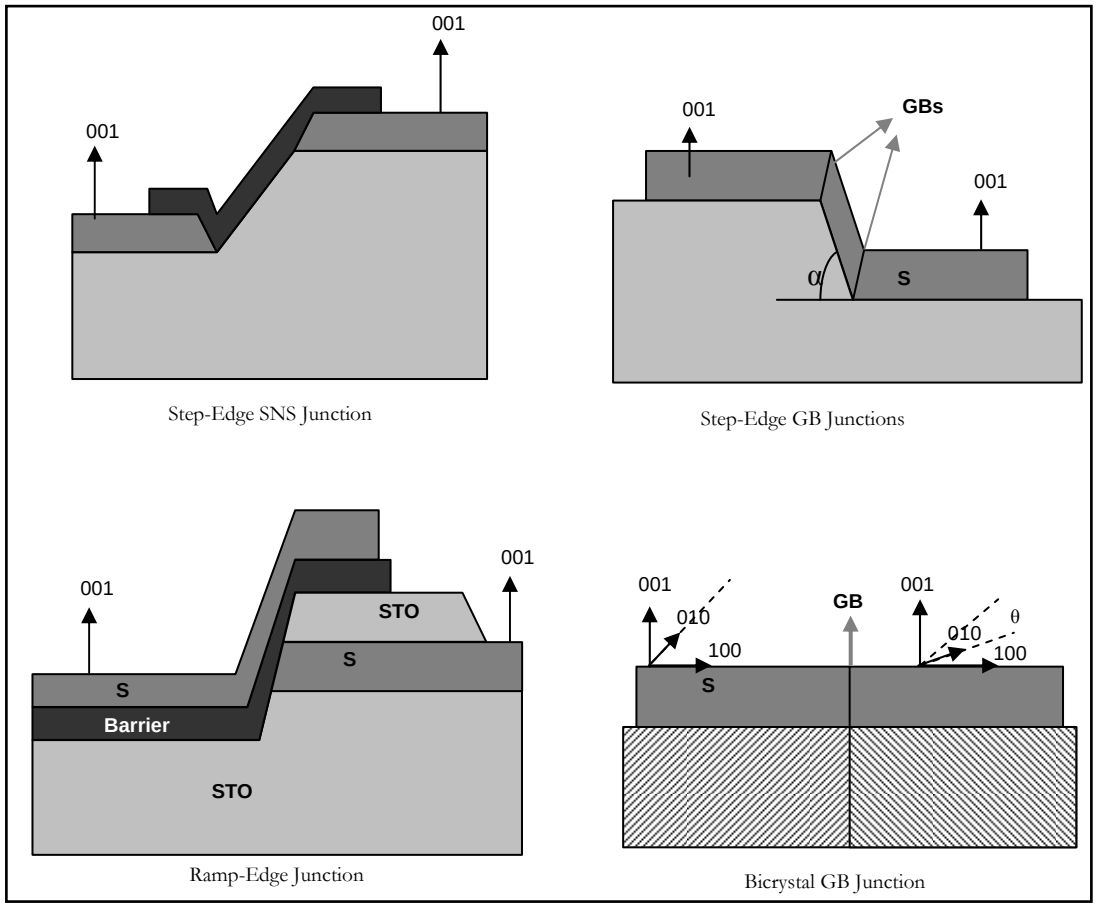

Figure 3.2. Grain boundary Josephson junction types. a) Step-Edge SNS Junction, b) Ramp-Edge Junction, c) Step-Edge GB Junctions, d) Bicrystal GB Junction (Source: Koelle 1999)

Owing to epitaxial growth, the substrate grain boundary is replicated in the film. This technique enables one to fabricate well-defined grain boundaries of many misorientations and to analyze their properties in direct comparison to those of the abutting grains (Hilgenkamp and Mannhartt 2002, Sarnelli and Testa 2001). In high-T_c

superconducting electronics, there are different types of grain boundaries which are usually classified into four types: step-edge SNS junctions, ramp-edge SNS junctions, step-edge grain boundary junctions, and bicrystal grain boundary junctions (McBrien 2000). According to the displacement and the rotation of the abutting crystals, as shown in the Figure 3.2.d, bicrystal GB junction types are used in this study with single layer YBCO.

3.3.1. Bicrystal Grain Boundary Interfaces

The development of a useful HTS-JJ technology and understanding of transport across the grain boundary was pioneered by the work on bicrystal GBJJs at IBM (Chaudhari, et al. 1988). A bicrystal GBJJ is fabricated by the epitaxial growth of a high-T_c thin film on a bicrystal substrate with a predetermined misorientation angle. The grain boundary is formed along a straight line running across the substrate. Hence, this technique is appropriate for SQUIDs or for other applications which do not require many junctions at arbitrary position on a chip.

Bi-crystal grain boundaries are created when a cuprate film is epitaxially grown on a suitable bicrystal substrate whose two crystal halves have some arbitrary relative orientation. The orientation of the overlying cuprate film is determined by the substrate crystal and the resulting grain boundary follows that of the substrate. The transport properties across the boundary are determined by the angle between the two grains. For small angles, $\theta < 10^o$ for YBCO, the grains are strongly coupled and the critical current density is limited by vortex motion along the boundary. For larger angles, the grains exhibit weak link behavior (Dimos, et al. 1990). The critical current decreases exponentially with increasing angle to a minimum at $\theta = 45^o$. This decrease is due to the anisotropic d-wave order parameter coupled with a faceted interface, dislocations, and band bending effects reducing the carrier density at the boundary (Dimos, et al. 1990).

The GBJJs were studied in this study grown on $SrTiO_3$ bicrystals. Fabrication of the junctions is described in Chapter 4.

3.4. The Properties of YBCO

YBCO whose critical temperature T_c was above the liquid nitrogen (77 K) temperature was discovered in 1987(Wu 1987). Before 1987, most of superconducting materials were characterized by a low critical temperature close to liquid helium

temperature 4.2 K. New high temperature superconducting cuprates with high T_c based on lanthanides, barium cupper oxides were then discovered and found useful for industrial applications.

YBCO structure which is shown in the Figure 3.3 consists of three perovskite unit cells stacked along the c-axis. The structure contains a layer of yttrium atoms sandwiched between copper oxide planes, followed by a barium oxide layer, copper oxide chain and another barium oxide layer. The oxygen content in YBCO determines the crystallographic structure, and the hole concentration in the CuO_2 planes. For an oxygen content $x=6$ (where$7-\delta$), the compound YBCO is in the tetragonal and an insulator. Increasing the oxygen content up to $x=6.6$ the compound undergoes a phase transition from tetragonal to orthorhombic (Jorgensen, et al.1987, Cogollo, et al. 2003 Gonzales 2005).

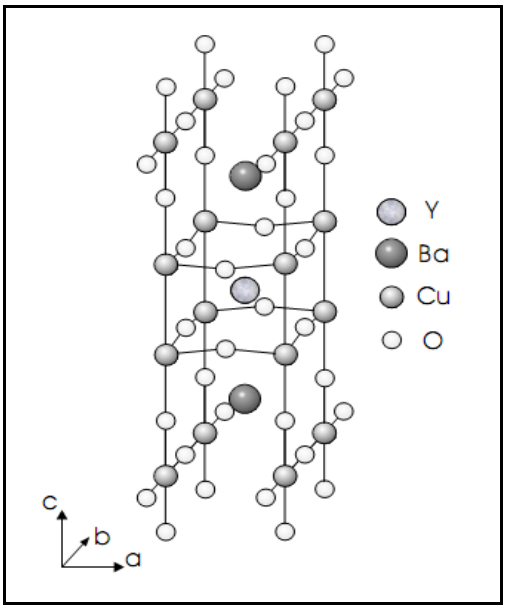

Figure 3.3. Crystal structure of YBCO orthorhombic phase
(Source: Neils 2002)

The critical temperature of YBCO is also strongly dependent on the oxygen doping. YBCO exist in either a tetragonal or orthorhombic crystal structure being only superconducting in the orthorhombic phase. YBCO has an orthorhombic room temperature phase with cell parameters $a = 3.828^{\circ}A$, $b = 3.888^{\circ}A$, and $c = 11.65^{\circ}A$. The tetragonal phase is only observed at high temperature in a range between 750 ^{o}C and 900 ^{o}C. On decreasing the temperature and increasing the oxygen content of the sample,

by oxygen uptake and diffusion, a second-order phase transition occurs at about 700 ^{o}C from the tetragonal to the orthorhombic phase.

Many approaches have been tried for practical devices based on $YBa_2Cu_3O_{7-\delta}$ (YBCO) which is the only material for developing the high-T_c electronics (Koelle, et al. 1999). In this section we will give a brief description about YBCO thin films, deposition techniques, and properties needed for high-T_c JJs.

YBCO material becomes superconductor at temperatures around 92 K, which is higher than the boiling point of liquid nitrogen (77 K). This allows tremendous developments in worldwide research on superconductivity and superconducting electronics, because the temperature for superconducting transition is very much easier to achieve, simpler, and cheaper with liquid nitrogen than that of liquid helium (4.2 K). Despite the wide variety of high-T_c compounds becoming superconductor in liquid nitrogen, work on SQUIDs has been restricted to YBCO due to its sufficiently strong pinning at 77 K, which is very important for achieving high critical current densities in *ab* plane and relatively low 1/f noise depending on the flux noise contribution caused by the hopping of weakly pinned vortices.

This is largely because, YBCO thin films are able to deposited successfully on variety of substrates due to its c-axis normal to the substrate showing acceptable pinning [Stephens 1991]. Furthermore, up to date YBCO thin films have been well understood to achieve high quality thin films. Although there are a number of different deposition techniques, pulsed laser deposition and sputtering are the most used techniques yielding high quality of films with very smooth surfaces and superior electrical properties.

Typically YBCO thin films, is grown with 200 nm thickness on well lattice-matched substrates such as $SrTiO_3$ (STO), have critical current density of (2-5) x10^6 A/cm^2 at 77 K. The c-axis property is characterized by the half-width of the x-ray rocking curve (005) has typically values of 0.10^0-0.30^0, and the surface roughness determined by atomic force microscope is around 10 nm.

The critical current densities in such films having above values are two orders of magnitude higher than in high-quality YBCO single crystals, indicating that a high density of defects, which provide strong pinning sites, must be present.

The JJs, described in this study are made of YBCO thin films, which fabricated by using magnetron sputtering. The fabrication methods and properties of the junctions will be described in the next chapters.

CHAPTER 4

EXPERIMENTAL TECHNIQUES

In this chapter, the experimental procedure which has been performed in the process of fabricating and characterizing Josephson Junctions were discussed as part of the work done towards completing this thesis. First section covers the general features of the fabrication process, while the second covers the stages of the device fabrication. The third section describes the measurement setup and the last section, details the techniques used for the characterization of the devices.

4.1. Device Fabrication

The steps below detail the process of device fabrication up to the measurement phase. The basic device fabrication steps can be listed as follows:

- Junction mask design,
- Substrate preparation,
- YBCO thin film deposition,
- Photolithography and Patterning,
- Etching,
- Contact Metallization (Gold Deposition).

4.1.1. Junction Mask Design

In order to fabricate Josephson junctions onto the grain boundary of the bicrystal substrates, special masks including different junction widths and shape were designed and produced as can be seen in the Figure 4.1. These masks consist of strip lines and meander pattern structures having width of 2 – 10 μm. Each mask contained different junction width and junction number in order to compare the junctions fabricated under same fabrication process. Junction masks were designed using L-Edit mask layout software and fabricated at Tubitak-UEKAE

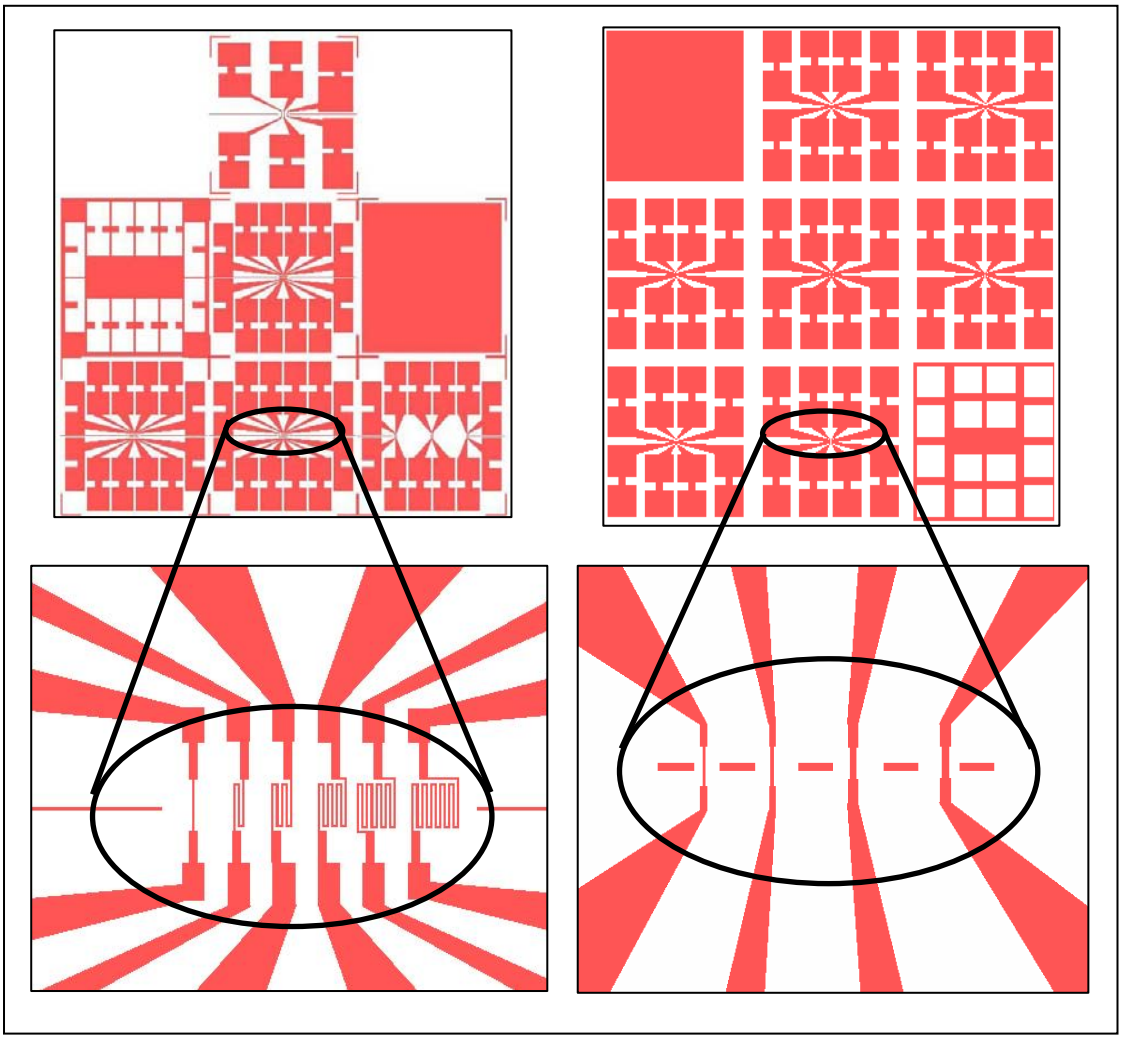

Figure 4.1 Josephson junctions mask layouts

4.1.2. Substrate Preparation and Cleaning

The choice of substrate materials is of primary importance for the development of a reliable junction technology onto the YBCO thin films. There are a number of substrates suitable for growing high quality YBCO films (Phillips 1996). To fabricate low noise Josephson junctions one usually chooses substrates that are closely lattice matched to YBCO and have comparable thermal expansion coefficients (Wördenber, 1998). The basic requirements for the substrates can be summarized as follows:

- Crystallographic lattice match between film and substrate
- Similar thermal expansivities of film and substrate
- No chemical interaction between film and substrate
- Suitably polished surface, stable and reasonably robust

All YBCO films used in this study were fabricated on commercially available 24 and 36 degree $SrTiO_3$ bicrystal substrates purchased from different manufacturers. The $SrTiO_3$ bicrystals are formed by fusing two single crystals together in the desired orientation forming a grain boundary. The fused crystals are then cut and polished to a 1cm × 1cm × 0.5mm size such that the grain boundary runs through the center of the substrate, parallel to one side. $SrTiO_3$ substrates are ideal for growing many cuprate materials due to the unit cell size being well matched. This ensures that the thin films will grow epitaxially with the underlying orientation of the substrate. A grain boundary will form in the thin film due to the mismatched orientation at the bicrystal grain boundary. Table 4.1 shows the unit cell spacing of $SrTiO_3$ along with the cell spacing of YBCO. The bicrystal substrates are very expensive and are thus reused when possible. Old patterned films are removed and the substrate can be used for another film deposition.

Table 4.1. The unit cell spacing for YBCO and $SrTiO_3$
(Source:Rajiv and Kumar 1998)

Material	Crystal Structure	Unit Cell Spacing		
		a(A)	b(A)	c(A)
$SrTiO_3$	cubic	3.90	3.90	3.90
$YBa_2Cu_3O_{7-\delta}$	orthorhombic	3.82	3.88	11.68

Substrate cleaning is a very important step of the process of deposition of thin film. Even a small dust particle on the substrate can prevent the formation of a homogenous thin film structure, resulting in faulty devices. Substrates must be as clean as possible before the deposition of the film. In order to clean the substrate the following steps were performed:

- Ultrasonic cleaning of the substrate in acetone for 30 minutes at 30 ^{0}C
- Ultrasonic cleaning of the substrate in alcohol for 30 minutes at 30 ^{0}C
- Drying of the substrate with N_2 gas

After proper cleaning, the substrate is ready for the deposition of the YBCO film on top of the substrate. Cleaned substrate is glued with paint silver onto the heater of the deposition system. This ensures good thermal conductivity between the heater and the substrate as well as good adhesion of the substrate to the heater.

4.1.3. Film Deposition by DC Magnetron Sputtering

Among the many different techniques used to deposit YBCO, the most common applied are pulsed laser deposition and sputtering. All of these techniques produce high quality YBCO films. In this study, sputter deposition techniques were utilized. Sputter deposition is a physical vapor deposition method of depositing thin films by sputtering a block of source material onto a substrate.

$YBa_2Cu_3O_{7-\delta}$ thin films were deposited by "in situ" DC inverted cylindrical magnetron sputtering (ICMS) system on (100)-oriented and $10\times10\times0.5$ mm^3-sized 24^0 and 30^0 bicrystal $SrTiO_3$ substrates. The target-substrate distance was optimized at 35 mm. Besides the deposition conditions, the cleaning of the substrate surfaces within the appropriate chemical solutions is a very important process for the epitaxial thin film growth as previously explained. The substrates were cleaned with an ultrasonic cleaner in acetone for 30 minutes and subsequently in isopropyl alcohol for 30 minutes. The substrates were attached to a Teflon holder with an angle of 45 degree. Then the ultrasonic cleaner was turned on while adjusting the temperature of the water inside to 30 ^{0}C. After cleaning, the substrate was glued to the substrate holder of sputter system with silver paint. The system was then sealed. The Ar partial pressure inside the chamber was adjusted to 0.5 mbar. The target was pre-sputtered in flowing Ar gas for 10 minutes under 45 W power during which the temperature of the sample holder was increased up to the deposition temperature of 780 ^{0}C. This pre-sputtering is required for eliminating any contamination on the surface of the target. At 780 ^{0}C, the oxygen gas was introduced into the chamber to attain the partial pressure of oxygen of 0.1 mbar and finally the total pressure inside the chamber was brought to 0.6 mbar.

At these conditions thin film deposition was started with fixed deposition parameters, namely, a total pressure of 0.6 mbar, a substrate temperature of 780 ^{0}C, and the dc sputtering power of 50 W. The resulting deposition rate was approximately 1.3 nm/min. After the deposition, pure oxygen was introduced into the deposition chamber with the partial pressure of 1 mbar while the temperature was fixed at 800 ^{0}C for 10 minutes. The temperature was then allowed to fall down to 600 ^{0}C at a rate of 20 ^{o}C/min. At the beginning of the cooling from 800 ^{0}C to 600 ^{0}C, oxygen pressure was increased up to 700 mbar and films were held at 600 ^{0}C for 20 minutes. Afterwards,

then the temperature was again allowed to drop, this time to the room temperature at a rate of 30 ^{o}C/min.

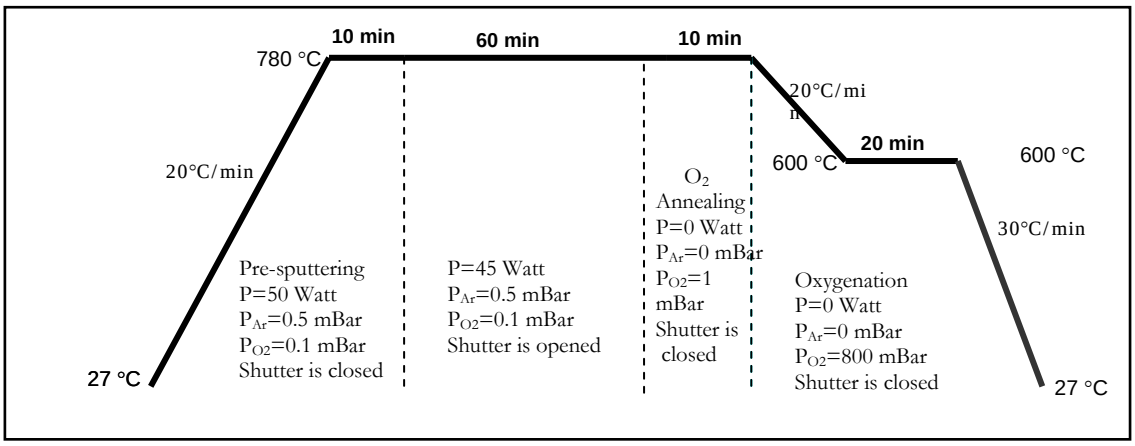

Figure 4.2. YBCO thin film deposition process

4.1.4. Photolithography Process

Photolithography is the process of transferring geometric shapes on a mask to the surface of a substrate or thin film. The steps involved in the photolithographic process are photoresist application; soft baking; mask alignment; exposure and development; and hard-baking.

Patterning techniques that are well established in semiconductor and LTS technology are not necessarily applicable to YBCO thin films. One immediate problem is that contact of YBCO with water or water-soluble chemicals degrades the superconducting properties (Avci, et al. 2007). Second, the use of dry-etching methods in a vacuum such as Ar ion beam etching can lead a significant heating of sample and thus to oxygen loss at the patterned edges. Even though these limitations, a number of techniques have been successfully used to pattern YBCO films down to submicron dimensions without degrading their properties (Braginski 1993).

As the first step of our patterning process, AZ5214 photoresist was applied on top of the YBCO layer which is deposited on $SrTiO_3$ substrate using home-made spinner shown in Figure 4.3 for resist coating. Spin coater works with a dc power supply, it surrounded with aluminum foil in order to prevent the sample in case releasing during spinning. Coating lasts for 90 second at 4000 rpm yielding a photoresist having a thickness about 1μm. This high-speed centrifugal whirling of

substrate is the standard method for applying photoresist coatings. This operation, known as, “Spin Coating", produces a thin uniform adherent, and defect-free layer of photoresist having correct thickness on the substrate or film surface.

Figure 4.3 Pictures of home made spinner used for photoresist coating

After covering the YBCO films with AZ5214 photoresist, they were baked for 3 minutes at 90^0C. This step is called soft baking, during which almost all of the solvents are removed from the photoresist coating. For baking a hot plate is used which can reach 90^0C in 5 minutes. Its temperature is controlled with a thermocouple. After reaching the desired temperature it stay almost stable during the baking process.

Soft-baking plays a very critical role in photolithography process. The photoresist coatings become photosensitive, or imageable, only after soft baking. Oversoft-baking will degrade the photosensitivity of resists by either reducing the developer solubility or actually destroying a portion of the sensitizer. Undersoft-baking will prevent light from reaching the sensitizer. Positive resists are incompletely exposed if considerable solvent remains in the coating. This undersoft-baked positive resists is then readily attacked by the developer in both exposed and unexposed areas, causing less etching resistance.

Figure 4.4. Picture of hot plate used for soft and hard baking

There are two types of photoresist: positive and negative. For positive resists, the resist is exposed with UV light wherever the underlying material is to be removed. In these resists, exposure to the UV light changes the chemical structure of the resist so that it becomes more soluble in the developer. The exposed resist is then washed away by the developer solution, leaving windows of the bare underlying material. The mask, therefore, contains an exact copy of the pattern which is to remain on the wafer.

Negative resists behave in just the opposite manner. Exposure to the UV light causes the negative resist to become polymerized, and more difficult to dissolve. Therefore, the negative resist remains on the surface wherever it is exposed, and the developer solution removes only the unexposed portions. Masks used for negative photoresist, therefore, contain the inverse (or photographically "negative") of the pattern to be transferred. In our study we used positive AZ5214 photoresist which is a widely used conventional photoresist. This photoresist also can be used as negative resist if the lithography process is properly changed for the negative photolithography. The figure below shows the patterning steps of YBCO Josephson junctions.

Once the soft baking completed the film is inserted to the mask aligner for the alignment of the mask on the grain boundary line of the substrate as seen in the Figure 4.5.

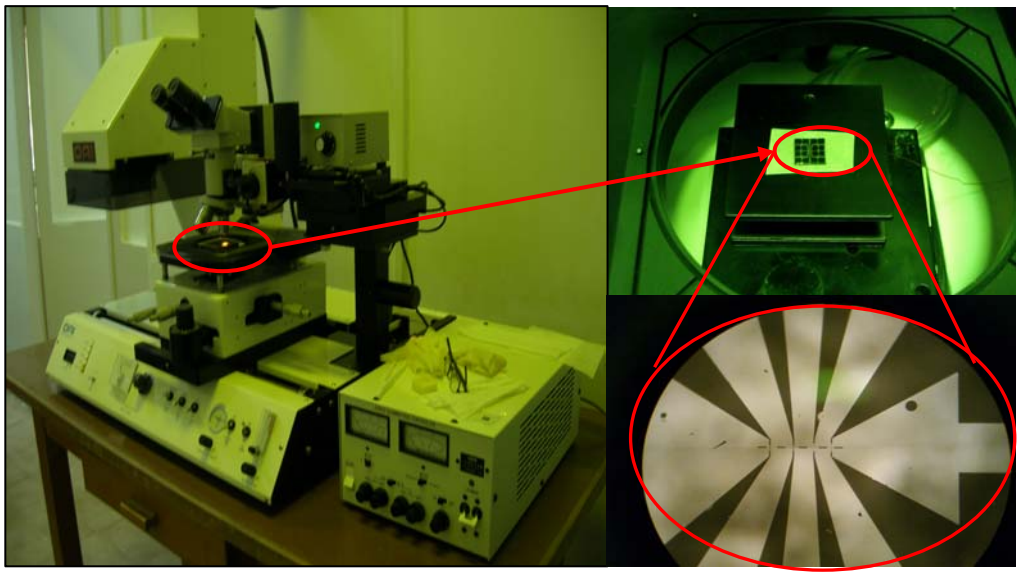

Figure 4.5. The pictures of OAI mask aligner having automatic controlled compact UV source, and patterned, Josephson junctions

Mask alignment is one of the most important steps in the photolithography process to fabricate a single layer Josephson junction one has to be able see the grain boundary line of the substrate to exactly align the mask. Also film structure and cleaning of the Josephson strip line area must be controlled during the alignment. A mask or "photomask" is a square glass plate with a patterned of Chrome film on one side. The mask is aligned with the substrate or film, so that the pattern can be transferred onto the surface.

Once the mask has been accurately aligned with the pattern on the grain boundary line of the substrate, the photoresist is exposed through the pattern on the mask with a high intensity near ultraviolet light (wavelength of 320 nm) during 45 seconds.

After the alignment and UV exposure step, the device pattern is coded in the photoresist as regions of exposed and unexposed resist.

The development process involves chemical reactions wherein unprotected parts of the resist get dissolved in the developer. A good development process has a short duration (less than a minute), results in minimum pattern distortion or swelling, keeps the original film thickness of protected areas intact, and recreates the intended pattern faithfully. We optimized the developing time for 30 seconds which produced excellent pattern on the film. During the development, it should always be followed by thorough

rinsing and drying to ensure that the development action will not continue after the developer has been removed from the film surface. We used de-ionized water for removing the developer and nitrogen gas for drying.

Development techniques are designed to leave in the resist layer an exact copy of the pattern that was on the mask. Problems resulting from a poor developing process are underdevelopment which leaves the incompletely developed the correct regions or a coved sidewall. In some cases, the development will not be long enough (incomplete) and will leave a layer or resist in the hole. The third problem is over development removes too much resist from the image edges or top surface.

Lithography process was completed with hard-baking. The temperature for hard baking was 105 ^{0}C for 5 minutes. This step is necessary in order to harden the photoresist and improve adhesion of the photoresist to the surface of the film.

4.1.5. Etching

In device fabrication, etching refers to a process by which material is removed from the substrate. There are two major types of etching: dry etching and wet etching. Wet Etching is an etching process that utilizes liquid chemicals or etchants to remove materials from the substrate, usually in specific patterns defined by photoresist masks on the substrate. Materials not covered by these masks are 'etched away' by the chemicals while those covered by the masks are left almost intact. A simple wet etching process may just consist of dissolution of the material to be removed in a liquid solvent, without changing the chemical nature of the dissolved material. In general, however, a wet etching process involves one or more chemical reactions that consume the original reactants and produce new species.

In our process, we used chemical etching process for YBCO thin film with an etchant of % 0.5 phosphoric acid (H_3PO_4). The etching time was optimized for 15 seconds and step by step process in order to avoid the under–etching during the long time immersion into the acid. However, sometimes we encountered the under-etch problem depending on the time, acid-DI water ratio, cleanliness of the beaker and purity of DI water as well as the acid. This is the general problems for chemical etch, but if the chemical are well prepared in a clean environment, and etching is carried out step by step controlled process, it mostly gives the devices with well patterned geometry.

Despite the resolution limitations of wet etching, it has found widespread use because of its following advantages: low cost, high reliability, excellent selectivity in most cases with respect to both mask and substrate materials. Automated wet etching systems add even more advantages: greater ease of use, higher reproducibility; and better efficiency in the use of enchants. Of course, like any process, wet etching has its own disadvantages. These include: limited resolution, higher safety risks due to the direct chemical exposure of the personnel, problems related to the resist's loss of adhesion to the substrate, and problems related to incomplete or non-uniform etching.

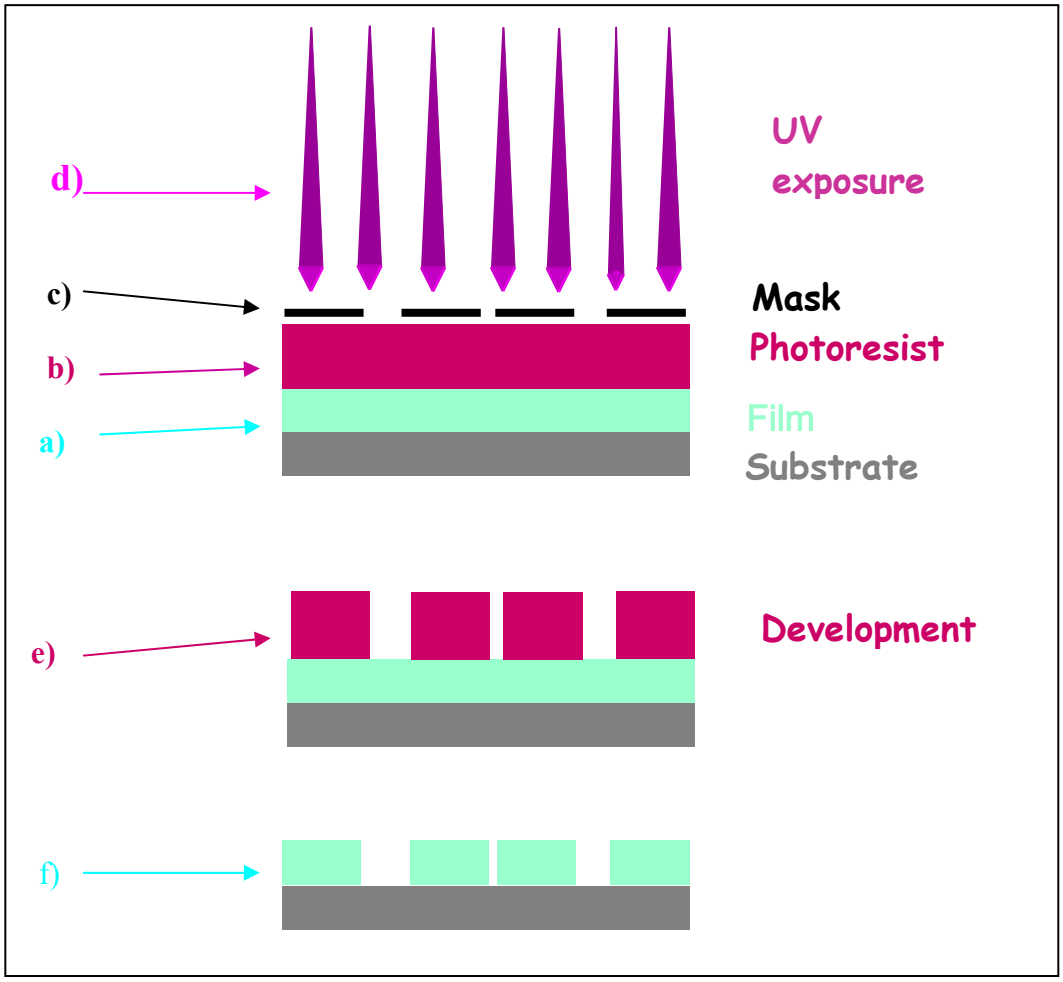

Figure 4.6. Photolithography process. a) YBCO thin film deposited on top of the STO substrate, b) Spin-coating of photoresist on top of the YBCO thin film, c) Chrome mask placement and alignment on top of the photoresist, d) UV exposure to photoresist through the chrome mask, e) Developing the photoresist, f) Etching of the YBCO film after lithography and subsequently removing the resist from the film surface

4.1.6. Contact Metallization (Gold Deposition)

The fabrication process was completed with the gold deposition on contact pads. At the room temperature a gold layer about 100 nm thickness was deposited on top of the contact pads of the junctions in order to prevent the device electrodes against the environment during a long storage. We have used Denton Vacuum Desk II etch-sputter unit and contact mask as seen in the Figure 4.7.

Gold layer deposition conditions: Gold contact pads are provided by means of dc-sputtering and structured with a lift-off technique. Before gold deposition, a negative mask is supplied by means of photolithography as described above. After gold deposition and photoresist removal the desired gold structure stays behind.

$P_{Ar} = 8.10^{-1}$ mbar

I = 20 mA (DC)

Target- Substrate distance =4 cm

Deposition time= 5 minutes.

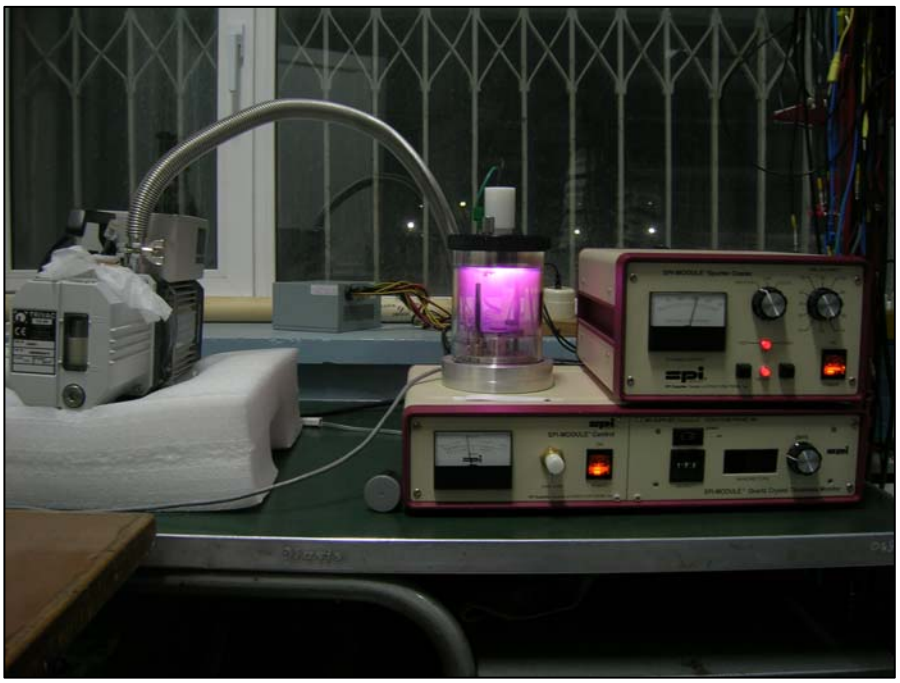

Figure 4.7. Sputter coater used for gold contacts

For the wire contacts we used two different techniques: First one is based on the so-called home-made wiring technique with the thin copper wire (0.08 mm diameter) glued with silver epoxy resulting in very low resistance (< 0.1 Ω) contacts at low temperatures. We used the thinnest copper wire for electronic contacts possible to decrease the thermal conduction between the room temperature and liquid nitrogen temperature via the wires. The second technique is based on the professional wiring by using the wedge bonder seen in the Figure 4.8. Using wire bonder gold wires were sticked on top of the gold contact pad with applying force. Optimization of bonding was performed by determining parameters for bonding time and force.

Figure 4.8. Wire bonder used for contacts

4.2. Measurement Setup

The films and devices were made subjected to microscopic and electrical analysis. The morphology of the surface was analyzed by scanning electron microscopy (SEM) and atomic force microscopy (AFM). The devices were electrically characterized by their resistance-temperature characteristics, magnetic susceptibility-temperature characteristics and current-voltage characteristics.

A characterization setup shown in the Figures 4.8 and 4.9 has been developed to investigate and measure electrical characteristics of the fabricated Josephson junctions mentioned above. The measurement setup was designed to be capable of performing resistance versus temperature, magnetic susceptibility and current-voltage measurements at liquid nitrogen temperature (77K). The techniques used for the characterization of the devices will be discussed in detail in the next section.

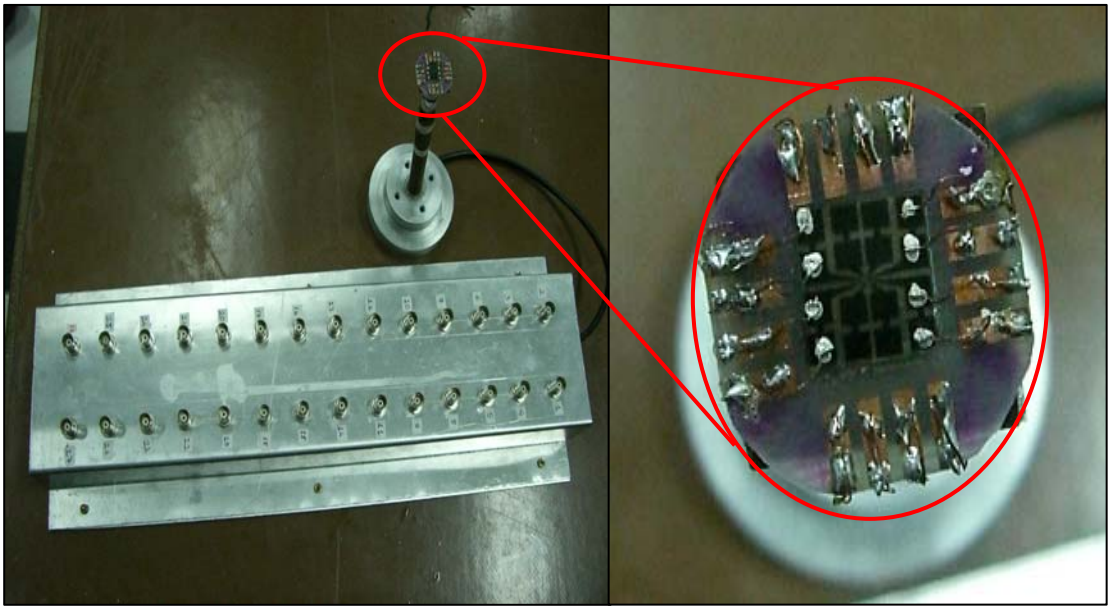

Figure 4.9. BNC box and junction probe designed to measure the junctions

In order to be capable of measuring all junctions on the same chip at the same time a junction probe were designed. Junction probe and BNC box were connected to each other with shielded cables. There are many advantageous of measuring the junctions at the same time. The junctions are immersed into the liquid nitrogen and there is no necessity of taking out of the probe for each junction. Hence, junctions are preserved form many thermal cycles between room temperature and liquid nitrogen temperature. This method is also very time efficient. All connections were done at the same time and junctions can be measurement one after another without taking out of the liquid nitrogen to room environment.

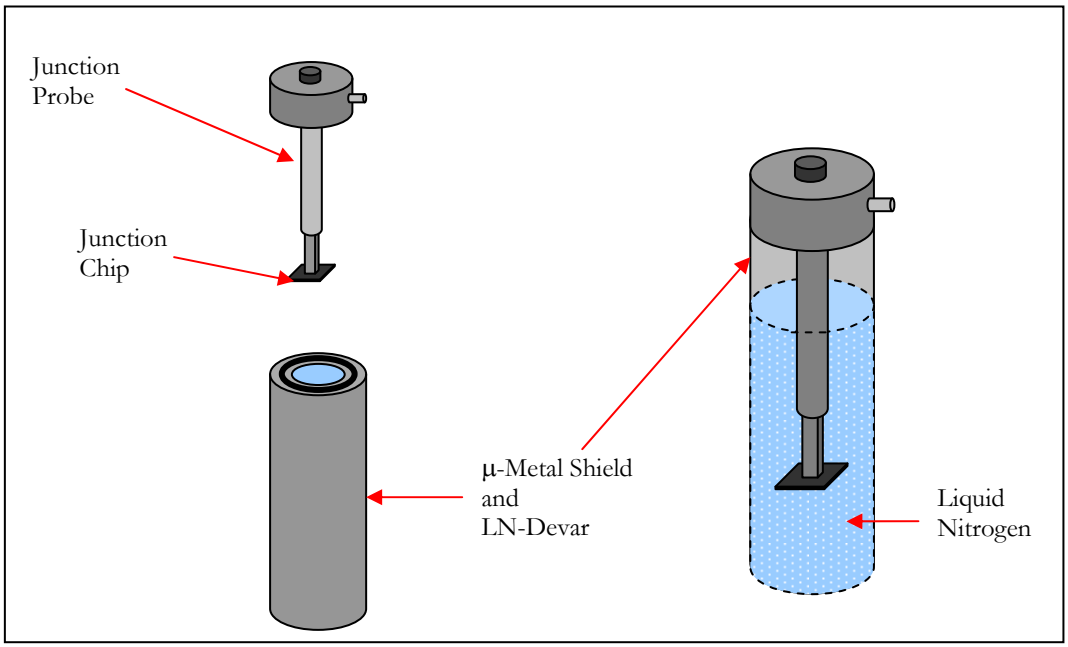

Figure 4.10. Electrical measurement setup used for obtaining current-voltage characteristics of the junctions and μ-metal shield implemented into the cryogenic dewar

Figure 4.10 shows the general view of the electrical characterization setup. For curren-voltage characterization above units were used as seen. For R-T and χ-T measurements a pyrex glass which can be vacuumed is used instead of the junction probe.

4.3. Characterization Techniques

4.3.1. Surface Characterization

Fabrication of high performance HTS Josephson junctions with controllable and reproducible parameters based on YBCO thin films requires a suitable technology. In order to obtain production parameters for such a device an investigation of the junction structural properties is required. Therefore, the study of the dependence of the transport properties of the junctions on the thin film deposition conditions is important in the understanding and application of high-T_c devices. A number of studies have been conducted on the optimization of YBCO thin film deposition conditions to achieve high reproducibility with desired superconducting properties. The critical current and the

structure of YBCO thin films have been studied to explain the current transport mechanisms depending on the pinning centers (Haage, et al. 1997).

Surface morphology measurements were made using SEM and AFM techniques in order to understand the effects of structural defects on the performance of the produced JJs. A brief explanation of said techniques follows.

4.3.1.1. AFM

Atomic Force Microscopy (AFM) is a useful method for the study of topographic surface features of epitaxial thin films. AFM is a local surface probing technique. The operation of an AFM is based on the detection of a low power laser beam reflected by the edge of a soft cantilever. The cantilever is typically made of silicon as the tip material and oscillates in free air at its resonant frequency. An AFM can operate in two principal modes, namely tapping (non-contact) mode and contact mode. The tapping mode operation is of advantage to investigate the sample surface state without its modification, where as the contact mode is used to add or remove atoms to or from the sample surface. There is also preference in using the tapping mode in order to record images of better resolution (Lee 2005).

In this study, AFM images of the fabricated films were taken in order to obtain information about the surface morphology of the films, hence improve the deposition parameter of thin films for the JJs. The AFM device used was a Multimode SPM, Nanoscope IV Digital Instrument with an ultra sharp tip which was operated in tapping mode. From 5 μm x 5 μm up to 100 μm x 100 μm area was chosen for AFM analysis of the junctions. The mean surface roughnesses of the films were found to range between 4 nm and 8 nm, depending on the deposition rate of the films.

4.3.1.2. SEM

Scanning electron microscopy (SEM) is a standard method used for characterization of the surface morphology of the thin films. This technique is very useful for a quick view of the entire surface area of a given film. More sensitive methods (AFM) are slower and allow investigation of only limited area of the sample. With SEM an electron beam scans the surface. The generated secondary electrons are

accelerated toward a detector. The pictures formed provide information down to submicron level.

In this study, SEM (Phillips XL-30S FEG) was used to analyze the surface of the films and substrates. SEM images of the films were taken at 38x, 100x, 120x and 50000x magnifications with 500μm, 200μm, and 500nm resolutions at the same operating voltage of 5keV.

4.3.2. XRD

X-ray diffraction (XRD) is a versatile technique used for identifying the crystalline phases present in the films and for analyzing the structural properties such stress, grain size, phase composition, crystal orientation and defects of different phases.

The θ-2θ XRD measurements were made by using a Philips X'pert Pro X-ray diffractometer with Cu-K_α λ=1.5418 A^0. The sample was exposed to angles θ between 10 and 60 degrees and reflected rays were detected at an angle 2θ with respect to the original beam.

4.3.3. Electrical Characterization

4.3.3.1. AC Magnetic Susceptibility Measurements

AC Magnetic susceptibility measurement is the standard tool for determining superconducting properties of the superconductors, such as the critical temperature (Xing, et al. 1993, Kunold, et al.2007). This measurement technique is based on the expulsion of magnetic field by the superconducting sample. A pair of coils is positioned on opposite sides of the superconducting thin film. Primary coil was biased with alternating current and generate magnetic field so that an inductance appears on the second coil. When the sample goes thorough the superconducting transition, the sample expels the introduced field, which can be seen by a distinct drop in the inductance of the coil. Analysis of the data reveals a sharp transition point at the critical temperature (T_c) of the magnetic susceptibility of the superconductor sample. In this study we have conducted susceptibility versus temperature measurements using the technique mentioned above.

In the normal state (above the critical temperature) superconductors typically have small susceptibility. In the fully superconducting state, the sample is a perfect diamagnet and so χ=-1. Typically, the onset of a significant nonzero χ' is taken as the superconducting transition temperature. By examining the peak location and the width of the peaks in the imaginary susceptibility it is possible to understand the behavior of the superconductivity in the weak links between grains in the sample.

The AC complex susceptibilities of the samples were measured via a two-coil system using a two phase SR830 Lock-in amplifier to pick up the signals of the secondary coil with AC magnetic field aligned perpendicular to the film surface. The excitation field within the primary coil was $h(t) = h_0 \sin 2\pi ft$ with a frequency of 1 kHz.

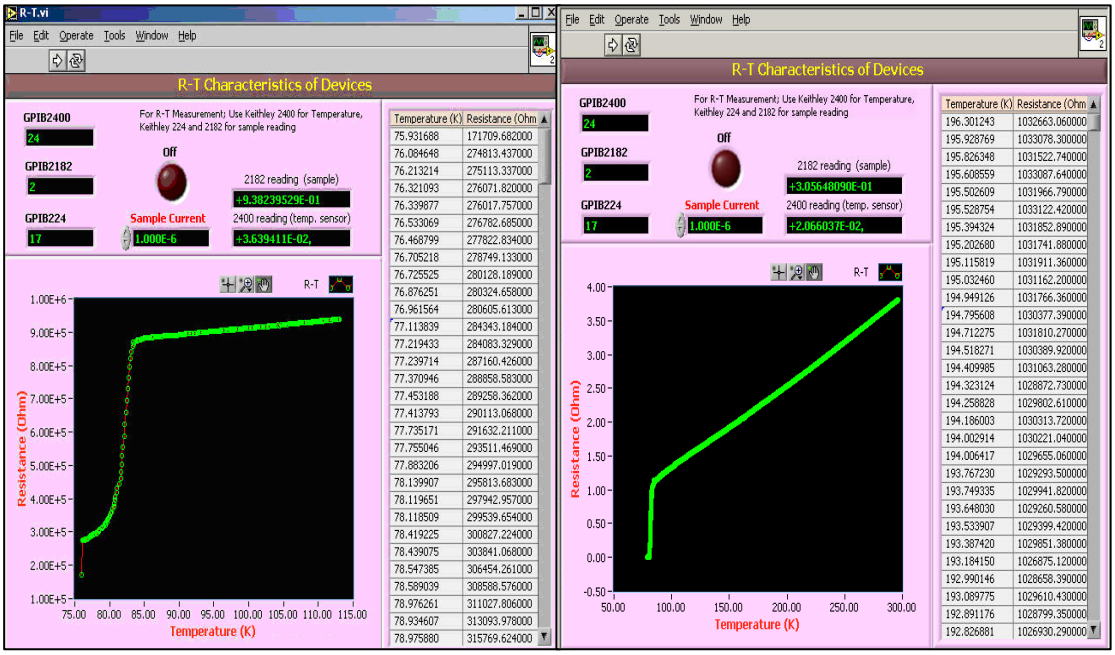

Figure 4.11. Labview program for χ-T and R-T measurements

4.3.3.2. Resistance-Temperature Measurements

In order to determine the transition temperature of the fabricated devices we performed electrical resistivity vs. temperature measurements as well as χ-T measurements. These measurements also provided us valuable information about the quality of the films. Four probe contact technique was used for the R-T measurements. The four point probe technique accurately eliminates the of contact resistance. In this technique, one applies the bias the outer contacts and measures the response from the

inner leads. In our study, the superconducting samples were current-biased and measured potential difference. It is generally more convenient to use current bias. Voltage biasing may be more accurate but is also requires a low noise current preamplifier for the measurement setup. The resistance is obtained from the ratio of voltage to current.

For the R-T measurements, a Keithley 2400 current source, a Keithley 2182 nanovoltmeter and a calibrated resistance (Pt-111) thermometer were used as part of the measurement setup. These devices were connected to a computer via a GPIB interface. A LabVIEW program was written for controlling the measurement setup as seen in the Figure4.11.

The samples to be measured were fixed on the sample holder with the help of some double sided tape. For the electrical connections, 0.08 mm copper wires were attached to the contact pads using silver paint. The sample holder was placed inside a specially made Pyrex glass tube which can be vacuumed was then slowly immersed into the liquid nitrogen dewar. A constant 10 μA bias current was applied to the current leads of the sample using Keithley 2400. The voltage cross the other leads of the sample was measured using a Keithley 2182 nanovoltmeter. The resistance values of the sample were calculated by dividing the current values to the voltage values, thus obtaining the R-T data.

Obtained resistance values of the Pt-111 were calibrated in terms of the corresponding temperature values of the samples. The resistance versus temperature values of Pt-111 is listed in the Table 4.2.

Table 4.2 Resistance-temperature values of the Pt-111.

Temperature (K)	Resistance (Ohm)
70.00	17.105
77.35	20.215
90.00	25.612
100.00	29.874
200.00	71.009
250.00	90.876
300.00	110.419

4.3.3.3. Current-Voltage Measurements

In order to obtain the current-voltage characteristics of our samples, contact pads of the junctions were covered with a gold layer, 0.1mm copper wires were then glued with silver paint to the contact pads of the devices using a 4-point technique. The current-voltage measurement system which consisted of a specially designed probe, a Keithley 2400 sourcemeter and a Keithley 2182 nanovoltmeter, was also computer controlled via GPIB interface using a program written in LabVIEW seen in Figure 4.12. The samples were current biased at various current values and the potential differences developed across the samples were measured. In order to diminish the influence of critical current fluctuations as well as to minimize the unwanted effects resulting from the electrical contacts and the voltmeter bias current reversal method was used.

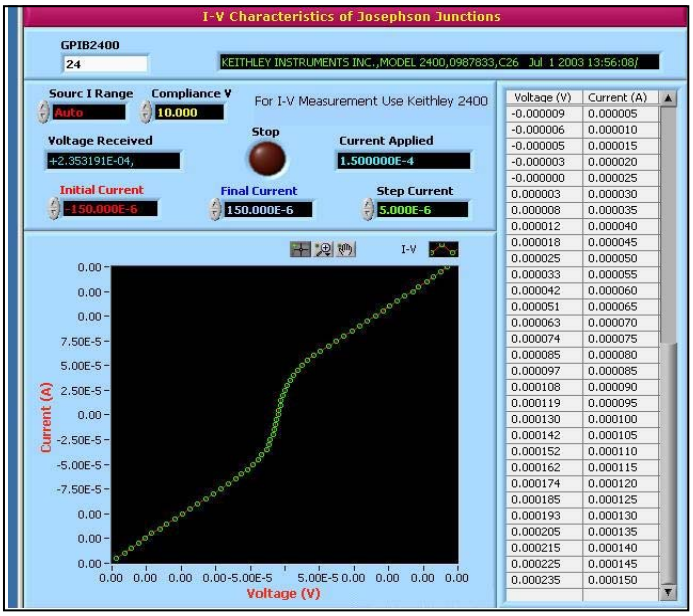

Figure 4.12. Labview program for I-V measurements

The junction probe was inserted into the μ-metal shield in order to eliminate ambient magnetic field effects coming from the environment. Before fully immersing the junction probe into the liquid nitrogen the samples were held for a few minutes above the nitrogen level inside the dewar in order to slow down the cooling of the sample, thus minimizing the formation of cracks between the leads and the contact pads. After immersing the junction probe fully into liquid nitrogen and waiting for a short

time for thermalization, a bias current was applied to the sample, with a typical range of -50μA and +50μA with an increment of 5μA. the range and step size were adjusted according to the properties of the junctions suc as critical current of the junction and the junction width. The I-V data was stored and plotted on the computer screen simultaneously with the measurement.

4.3.3.4. Critical Current-Magnetic Field Measurement

In order to measure the effect of magnetic field on the critical current of the sample, measurements were performed inside a 2-layer μ-metal shield as shown in Figure 4.13. The dc field was produced by a calibrated solenoid was applied perpendicular to the surface of the sample. The coil was inserted inside the dewar while is dewar full of liquid nitrogen after wires of the coils and nitrogen were thermally balanced junction probe were then immersed into the liquid nitrogen in the middle of the coil. Applying a dc current to the coil a magnetic field obtained perpendicular the junction chip, under this field magnetic field measurements were performed. The magnetic field dependence of the critical current was measured. The I_c vs. B ($I_c(B)$) plot of the junctions in this work revealed a well-defined Fraunhofer pattern like behavior.

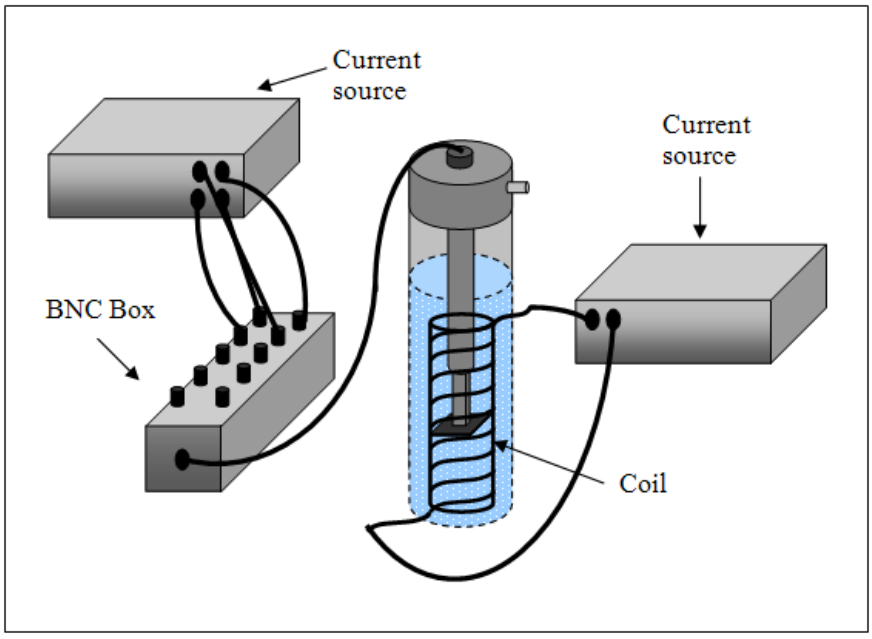

Figure 4.13. Magnetic field dependence measurement setup

CHAPTER 5

RESULTS AND DISCUSSION

In this chapter, experimental results for the Josephson junctions are given and the characterization features are explained briefly using theoretical predictions of the device properties. High temperature superconducting Josephson junctions, which are based on the bicrystal grain boundary junction technology, were fabricated onto YBCO thin films by using the method described throughout this thesis. The substrate materials were chosen as commercially available 24- and 30-degree 10x10x0.5mm^3 (100) $SrTiO_3$. The junctions were characterized systematically with respect to the device performance and optimization process depending on the fabrication concept.

200 nm thick YBCO thin films were deposited using a dc Inverted Cylindrical Magnetron Sputtering (ICMS) technique and the superconducting properties of the thin films were determined by electrical and magnetic characterizations consisting of the resistance versus temperature (R-T) and magnetic susceptibility versus temperature (χ-T) measurements, and structural properties were investigated by AFM, SEM and XRD analysis.

5.1. Resistance-Temperature Measurements

R-T measurements were performed on YBCO thin films before the device patterning. The samples were cooled from room temperature (~300 K) to liquid nitrogen temperature (77 K) and the superconducting transitions were observed determining critical temperatures, T_c. The R-T curves of the samples in their normal state between room temperature and T_c, having a slope passing very close to the origin as expected for a metallic normal state. The resistive behavior of the samples were typical for superconducting YBCO thin films. R (T) curves of the films deposited throughout this study were obtained as showing almost the same behavior having sharp transitions (ΔT~0.5 K) and the transitions were observed at 89-91 K with slight variations in T_c.

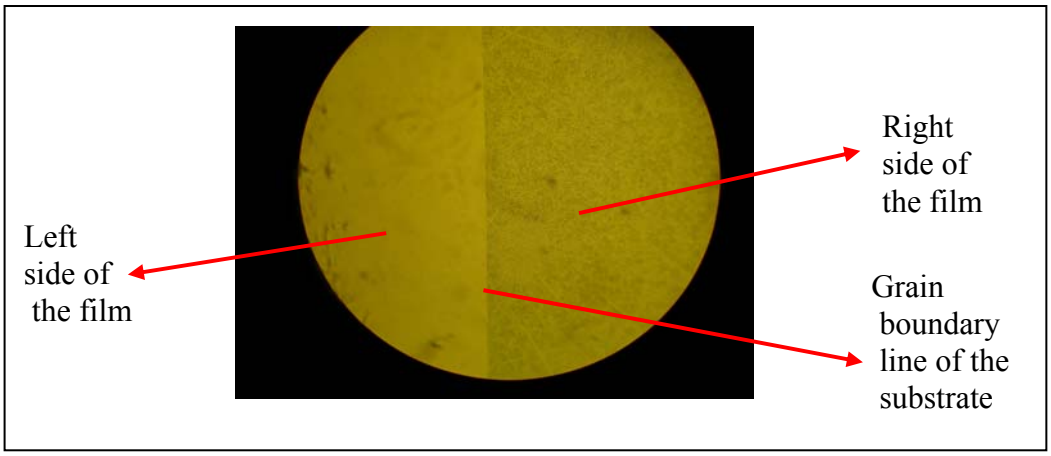

Figure 5.1. Optical microscope image of YBCO thin film

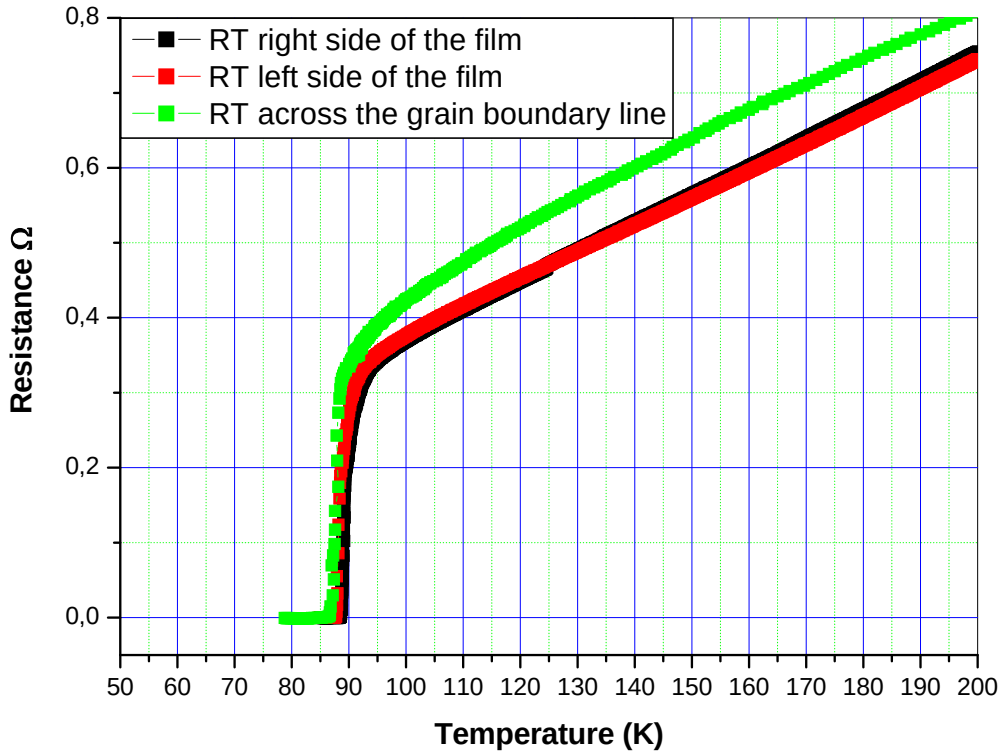

Figure 5.2. R-T graph of 24 degree bicrystal substrate across the grain boundary line and two sides of the line

Figure 5.2 shows the temperature dependence of the resistance of one of the YBCO thin film samples deposited on a 24-degree bicrystal substrate. Different curves represent the resistance across different part of the same film. The green curve shows

the R-T dependence of the film across the grain boundary line, the black one represents the R-T measurement of the right side (and thus does not include the effects of the boundary), and the red one is that of the left side of the grain boundary of the film. As seen in the graph that two sides of the film show the same transition temperature of 88 K with transition width of $\Delta T \sim 1$ K, which indicates the homogeneity of the film on the sides of the boundary. The measurement across the boundary line has relatively larger resistance above the critical temperature due to the boundary resistance contribution.

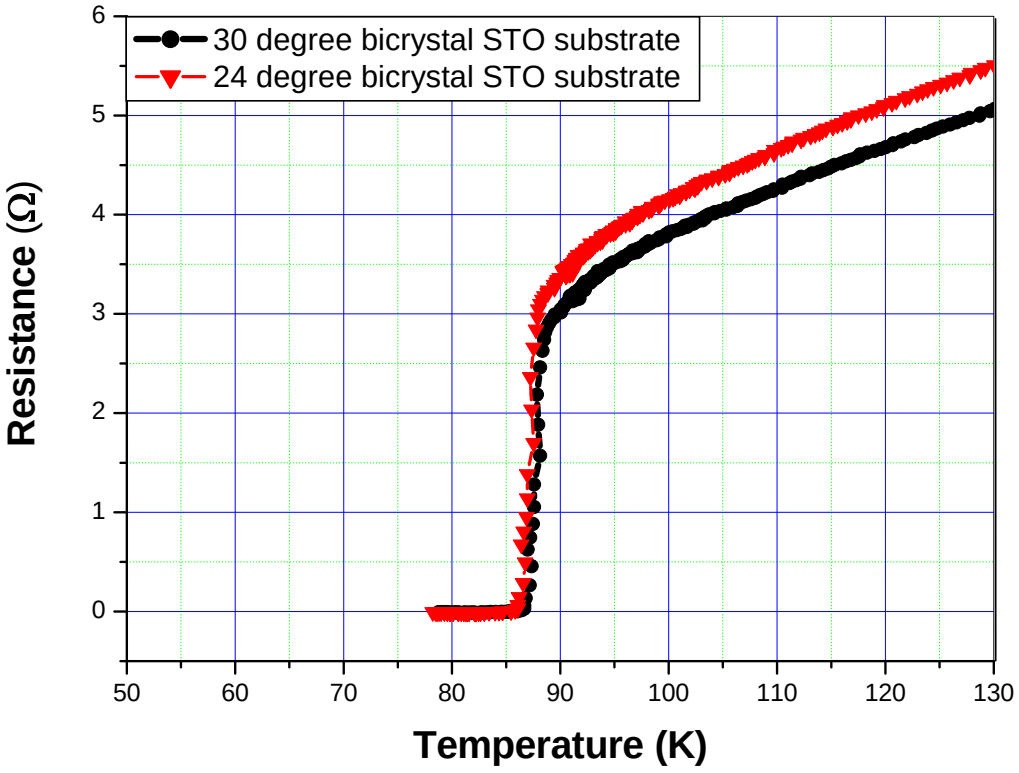

Figure 5.3. R-T curves of YBCO thin films across the grain boundary lines of 24- and 30-degree STO bicrystal substrates

Figure 5.3 shows the R-T characteristics of thin films deposited on the two different bicrystal substrates having 24- and 30-degree misorientation angles that we used during this study. These samples on these substrates showed almost the same transition temperature as expected for homogeneously deposited films.

5.2. AC Magnetic Susceptibility-Temperature Measurements

The AC magnetic susceptibility responses of the films for an applied magnetic field are depicted in Figure 5.4. The real part of susceptibility, χ', was observed to be step-like transition as a function of temperature, representing the near-perfect screening of complete penetration of external ac magnetic field into the sample.

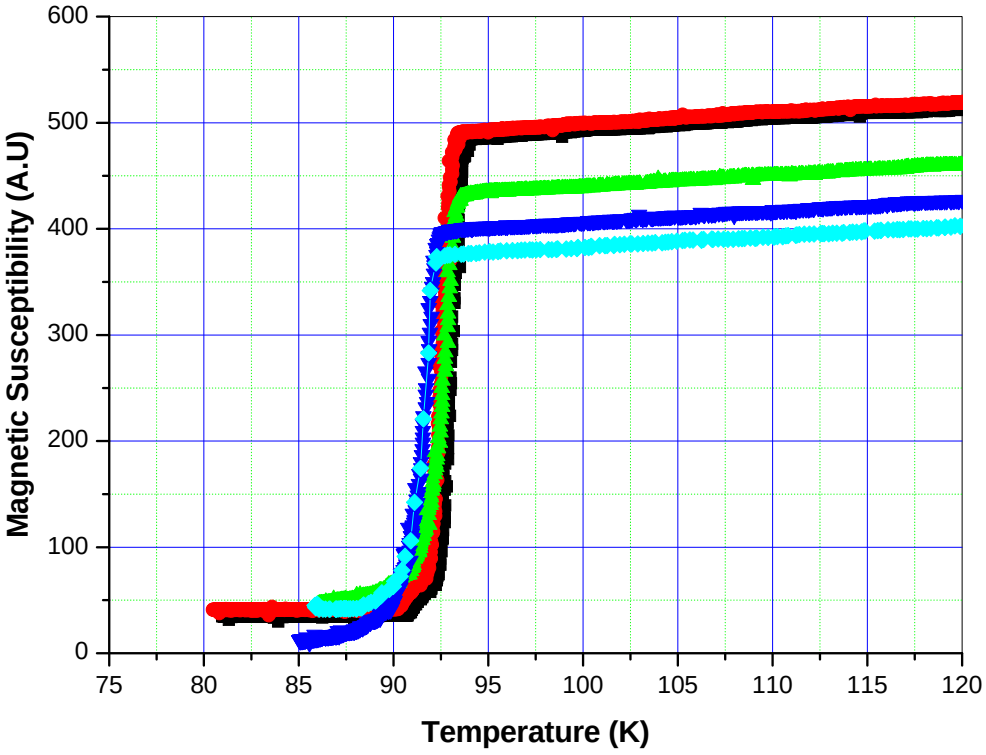

Figure5.4. Temperature dependence of magnetic susceptibility of different samples

Ac magnetic susceptibility responses of different films deposited under the same deposition conditions are similar with each other as of that in the resistive transitions. The sharpness of the transitions in Figure 5.4 indicates the strong diamagnetic properties of the homogeneous superconducting films.

5.3. Structural Analysis

X-ray diffraction patterns were employed to characterize to epitaxial growth and determine the crystal structure of the films. The full width at half maximum (FWHM) values measured from rocking curves of the YBCO (005) peaks whose values between 0.22^0- 0.28^0 show highly c-axis orientation in the film crystalline structure. XRD patterns of the YBCO thin films grown at optimized growth parameters are shown in Figure.5.5.

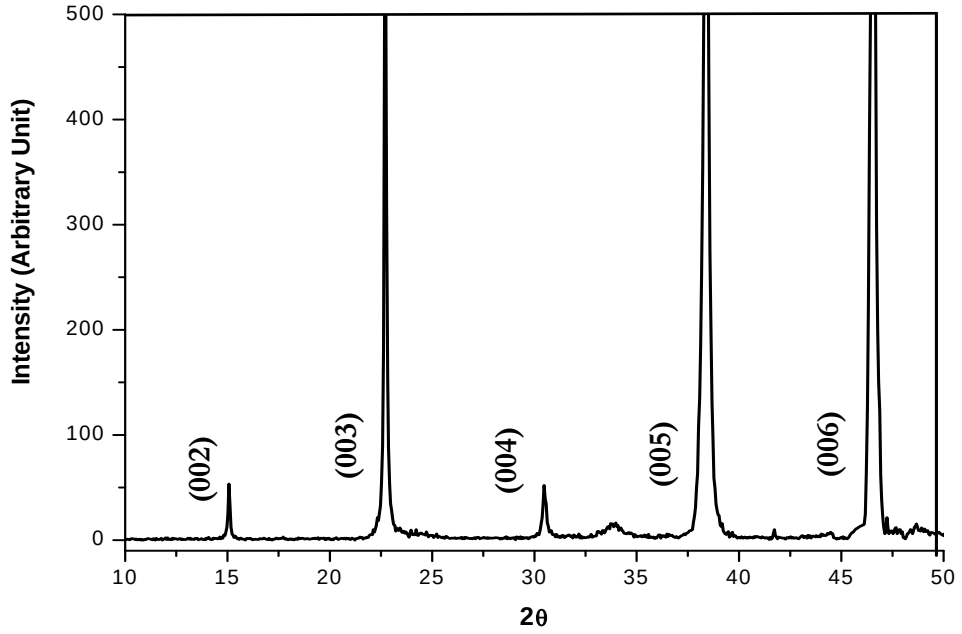

Figure 5.5. XRD peaks of YBCO Thin Films

The surface roughness of the films is an important parameter which affects the junction performance by means of the transport properties. As seen in Figure 5.6, the different samples showed different degrees of roughness and these values between 4 and 10 nm which are acceptable for YBCO thin films.

The AFM analyses were used to provide information on the success of the photolithographic procedure by means of surface morphology of the grain boundary region of the junction strip lines. Sharpness of the strip line edges shows whether there is a need for improvement of the lithographic process. Figure 5.6 shows the AFM images taken from the grain boundary region of the substrate after the film deposition and success of the lithographic process.

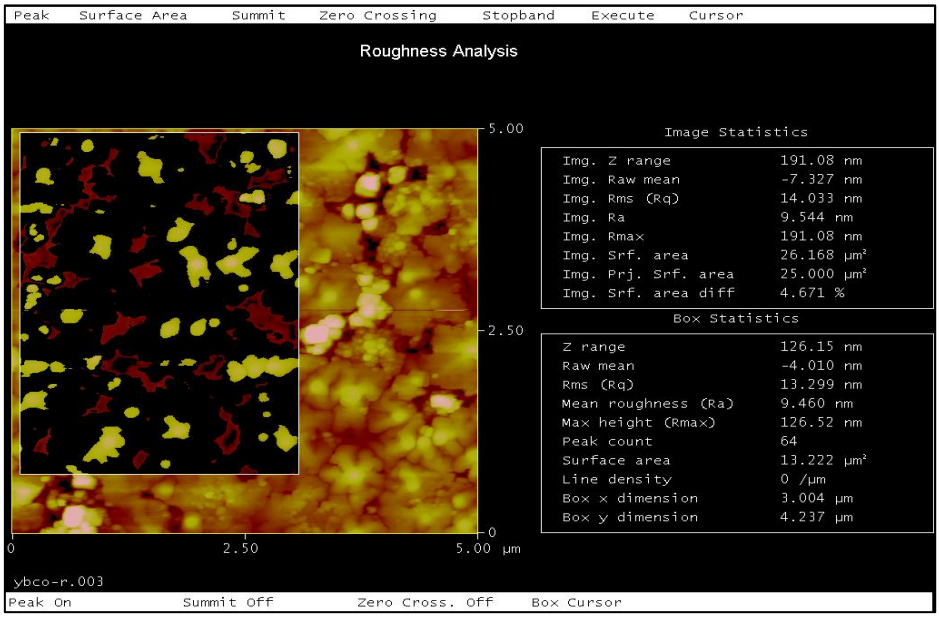

Figure 5.6.a. Roughness analyses of the junction strip line

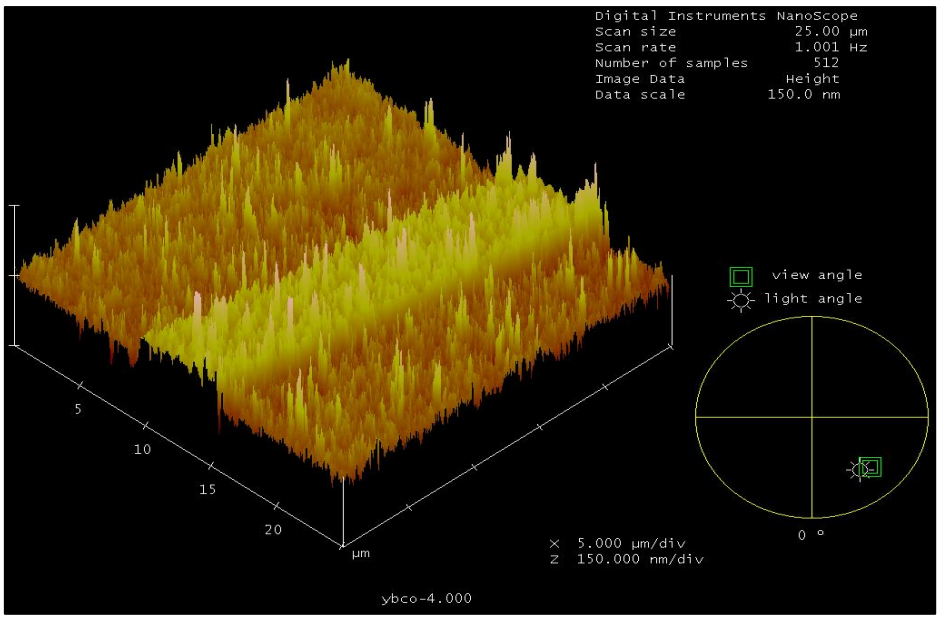

Figure 5.6.b. Junction profile

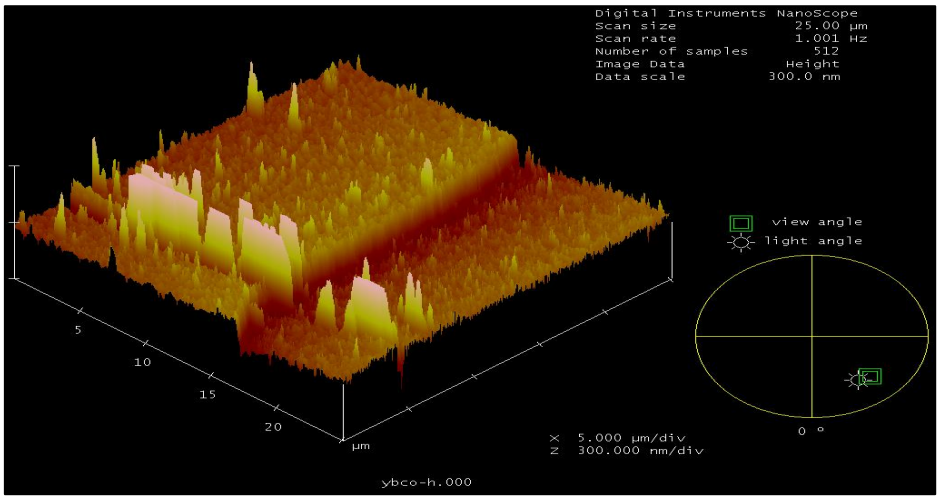

Figure 5.6.c. Edge profile of the junction

The roughnesses of our films are in the range of 4-10 nm which are typical for the device quality thin films due to the structural homogeneity over the grain boundary line, defect density, overall size of pin holes and their distribution over the film. The roughness analysis was performed on the strip line of one of the junctions of the chip. Figure 5.6.b shows the junction width of 5 µm. Figure 5.6.c shows the edge profile of the junction due to the patterning process.

The SEM images in Figure 5.7 show the pattern of junctions and grain boundary line of bicrystal substrate. We used the SEM analysis for determining the patterning results and geometry including the junction dimensions and placement of the strip lines onto the grain boundary line.

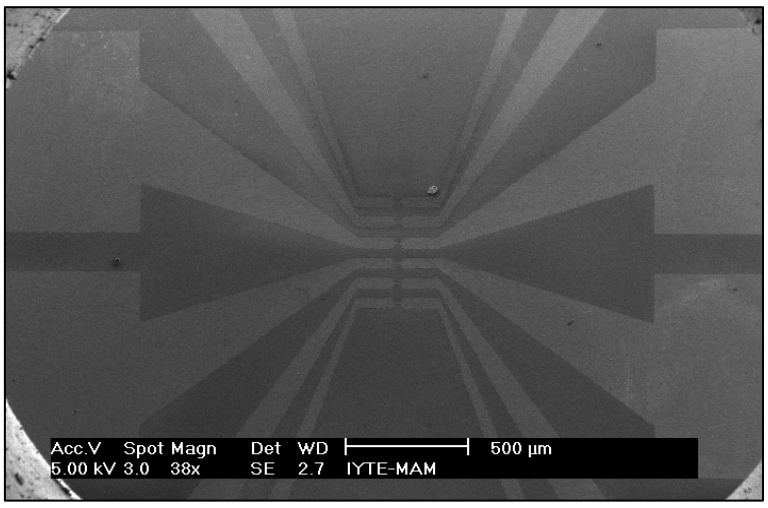

Figure 5.7.a. SEM image of the junction pattern

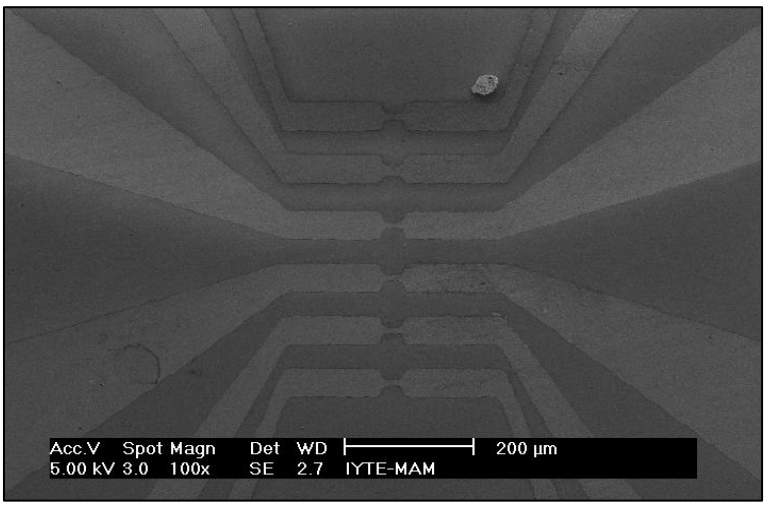

Figure 5.7.b. SEM image closer view of the junctions

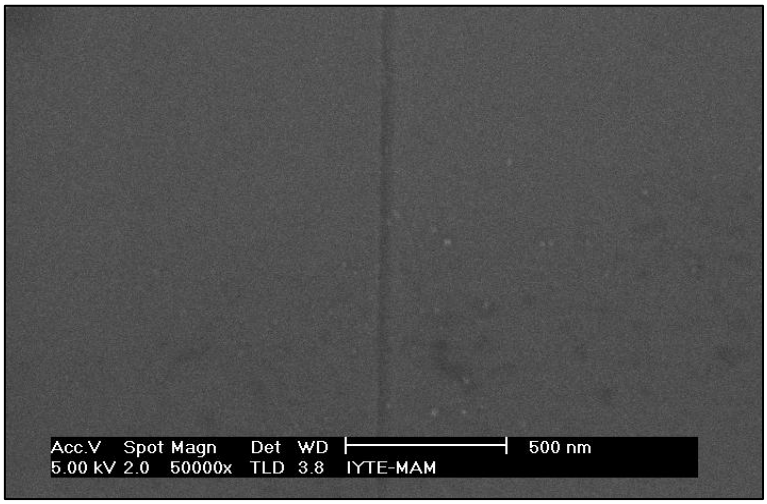

Figure 5.7.c. SEM image grain boundary line of the 24^0 bicrystal STO substrate

5.4. Current-Voltage Characteristics

The current-voltage characteristics of the JJs were performed both under zero applied field in magnetically shielded environment and with a magnetic field at 77 K as described in the sections 4.4.3.3 and 4.4.3.4.

I-V characteristics showed that the properties close to the predictions of the RSJ model having the critical currents I_c = 10-90 µA and normal resistances $R_n = 1-2\Omega$ with the product of I_cR_n = 40-100 µV. The variation on these values from device to

device is mostly caused by the effect of chemical etch, resulting the different junction widths and degrading the electrical properties of thin film due to the water inside. In all devices, the junctions were designed to have between 3 and 10 μm widths, however, sometimes this can be vary depending on the etching conditions.

The Josephson junctions fabricated on 24-degree STO bicrystal substrates can be show different characteristics on different devices although they are produced at the same optimized conditions because of the placement of the junctions on grain boundary line. The uniformity and surface morphologies of thin films deposited on top of grain boundary line of the substrates play important role on the I-V characteristics. These properties mostly differ for the different substrates purchased from different manufacturer. Therefore, the substrate condition is also responsible for the junction quality as well as the fabrication process. Our junctions have almost similar characteristics as in Figure 5.8.

I-V characteristics of our junctions were characterized depend on three main parameters which are bicrystal substrate orientation consisting of 24- and 30-degree, junction width consisting of 3, 5, 8 and 10 μm, and deposition rate between 1 and 2 nm/min.

5.4.1. I-V Characteristics in the Absence of a Magnetic Field

In Figure 5.8 and 5.9 current–voltage characteristics of our YBCO junctions measured at 77 K are shown. It can be seen from the graphs that up to the critical current I_c, no voltage can be measured across the sample. If the bias current is further increased, the normal conducting state is reached when the charge is mainly carried by normal electron, through the grain boundary line. From the slope of the current–voltage characteristics, normal state resistance (R_n), of the junction can be estimated. When decreasing the bias current after the junction has switched, the voltage at the junction switches again to the superconducting state with no voltage across the junction. For negative bias current exactly the same behavior is observed because of our junctions are non-hysteretic.

I-V characteristics of the JJs fabricated on bicrystal STO substrates having 24 and 30 degree orientations were compared. In the Figure 5.8.a and Figure 5.8.b I-V

characteristics for the 3, 5, 8 and 10 μm wide junctions fabricated on 24 degree and 30-degree STO bicrystal substrates are presented.

Many groups have measured the current carrying properties of grain boundaries prepared by the bicrystal technique. Their data showed that critical current of JJs is a function of misorientation angle θ. The critical current decreases as θ increases. Many attempts have been made to explain the decrease in I_c with increasing θ. Such a change is expected in a superconductor with d-wave symmetry, in which the strength of the superconducting coupling is orientation-dependent (Dimos, et. al 1988). When my results are compared with the literature related with decrease in I_c as the θ increase it can be seen that they are in agreement with each other. It can be seen from the graphs that with the increasing misorientation angle of bicrystal substrate from 24- to 30-degree, I_c values of the junctions tend to decrease. This is because the strength of the superconducting coupling across the grain boundary is a function of the misorientation angle defining the grain boundary.

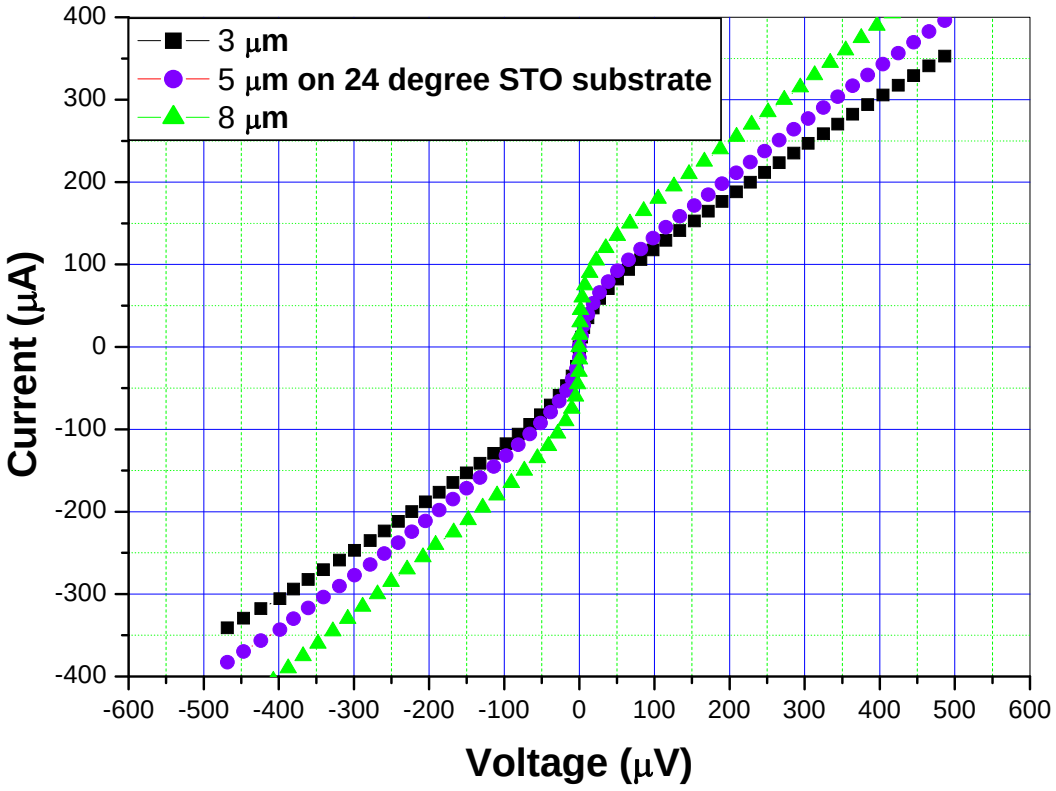

Figure 5.8.a. I-V characteristic of junctions on 24-degree bicrystal STO substrate

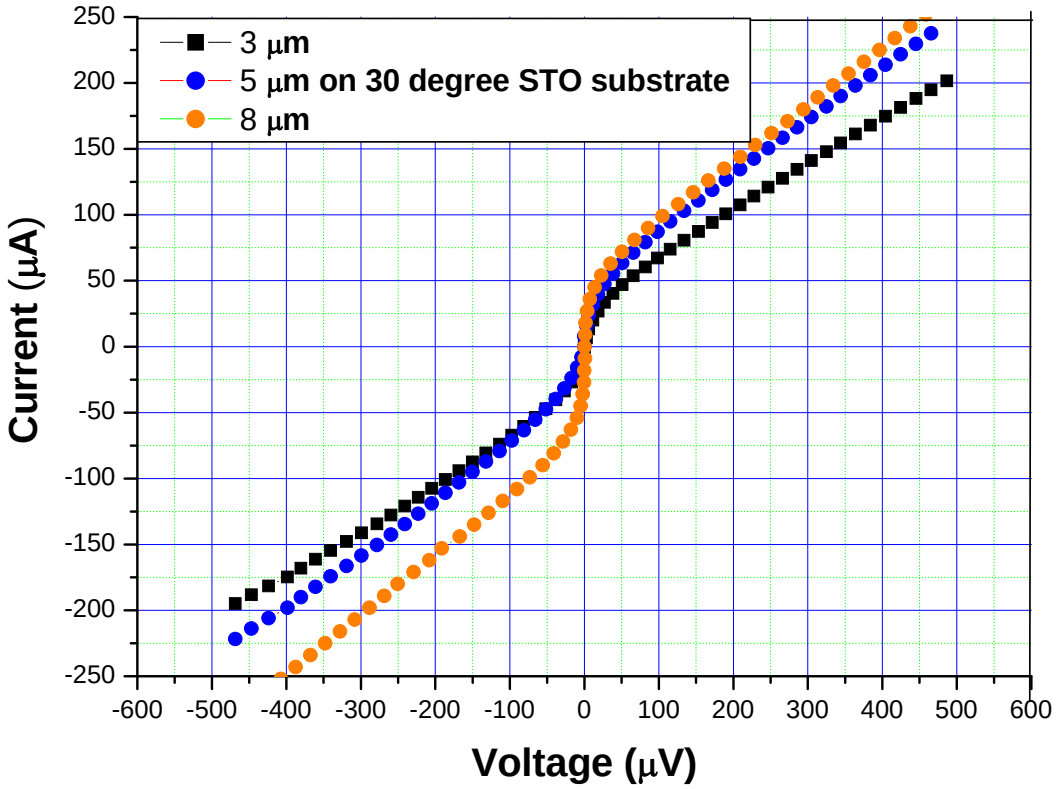

Figure 5.8.b. I-V characteristic of junctions on 30 degree bicrystal STO substrate

I-V characteristics showed that for two different bicrystal substrate orientations, the properties close to the predictions of the RSJ model having the critical currents I_c=25-90 μA for 24 degree substrate and I_c=10-40 μA 30 degree substrate. K. The R_n of the junctions also scaled inversely with the I_c for different junction widths, leading to almost similar I_cR_n values for the junctions on the same chip. The R_n of the 3, 5 and 8 μA wide junctions were measure to be about 1-2 Ω, respectively, leading to I_cR_n= 100μV. This is within the range of the reported values for this type of the junctions. Similar I_cR_n values for all junctions on a single chip were obtained, but they varied from one chip to another, indicating high sensitivity of the junction parameters to the film growth and the substrate GB structures. The variation on these values from device to device is mostly caused by the effect of the chemical etching process, resulting in the different junction widths and degrading the electrical properties of thin film due to the moisture.

5.4.2. Width Dependence of Josephson Junctions

The Josephson junctions with different widths were designed and created in order to investigate the effect of junction width on critical currents I_c, normal state resistance R_n and of I_cR_n product. Josephson junctions having widths between 3 and 10 μm were patterned on 24-and 30-degree $SrTiO_3$ bicrystal substrates Figure 5.9 shows the I-V characteristics of the junctions with different junction width fabricated on 24-degree bicrystal STO substrate.

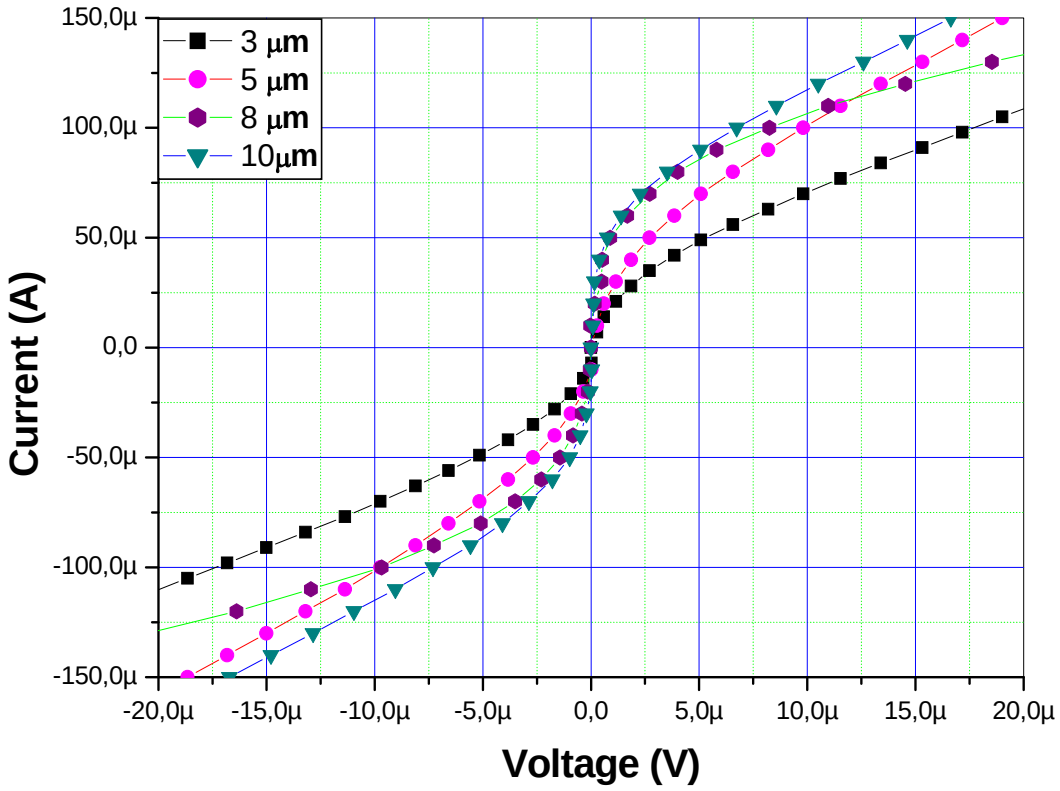

Figure 5.9. Junction width dependence of the I-V curves on a) 24-degree, b) 30-degree bicrystal STO substrate

While the I_c of the junctions made on the same chip decreased as the junction width decreased, a systematic change of the I_c versus the junction width was not observed. The I_c decreased much further than the junction width ratios. This is interpreted to be due to the defects at the junctions which would have more effect for the smaller junction width, effect of chemical etch, resulting the different junction widths and degrading the electrical properties of thin film due to the water inside and the uniformity and surface

morphologies of thin films deposited on top of grain boundary line of the substrates play important role on the I-V characteristics. The defects at the bicrystal GB junctions in our samples are thought to be mainly caused by the optically observed imperfection of the substrate GB deteriorating the growth of the film at the junctions.

5.4.3. Magnetic Field Dependence of Josephson Critical Current

The effect of applied field, B, on the I_c of the junctions was investigated in order to determine the magnetic field characteristics of the junctions. A classical magnetic field dependence of I_c of JJ is shown in the Figure5.10 for GBJJ of 4μ width. Magnetic field measurements were performed inside 2-layer μ-metal shield. The dc field was produced by a calibrated solenoid. $I_c(B)$ was measured in a magnetic field normal to the substrate. The I/I_c versus B plots of the junctions in revealed a well-defined Fraunhofer pattern like behavior which scaled with junction widths. The field dependence of the I/I_c of three junctions with widths of 4 μm at 77 K is shown in the Figure 5.10.

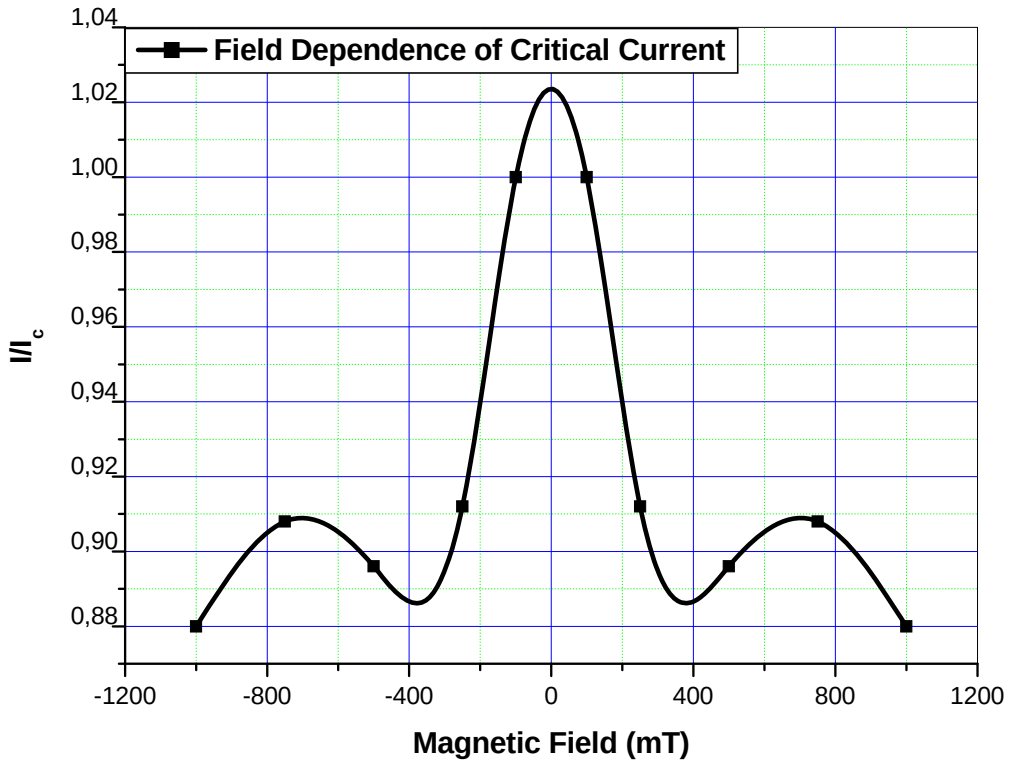

Figure 5.10. Magnetic field dependence of Josephson junction with 4μm width on 24-degree bicrystal substrate

5.5. Optimization Process of Josephson Junctions

We performed some optimization process for the Josephson junctions in order to improve both the signal performance and the stability of our devices against thermal cycle. The optimization process consists of several steps starting from the film deposition up to fabrication stage and measurement conditions as well. We obtained more reliable and stable junctions after these steps and we are giving the process in the following sections with obtained results.

5.5.1. Deposition Rate Dependence of Josephson Junctions

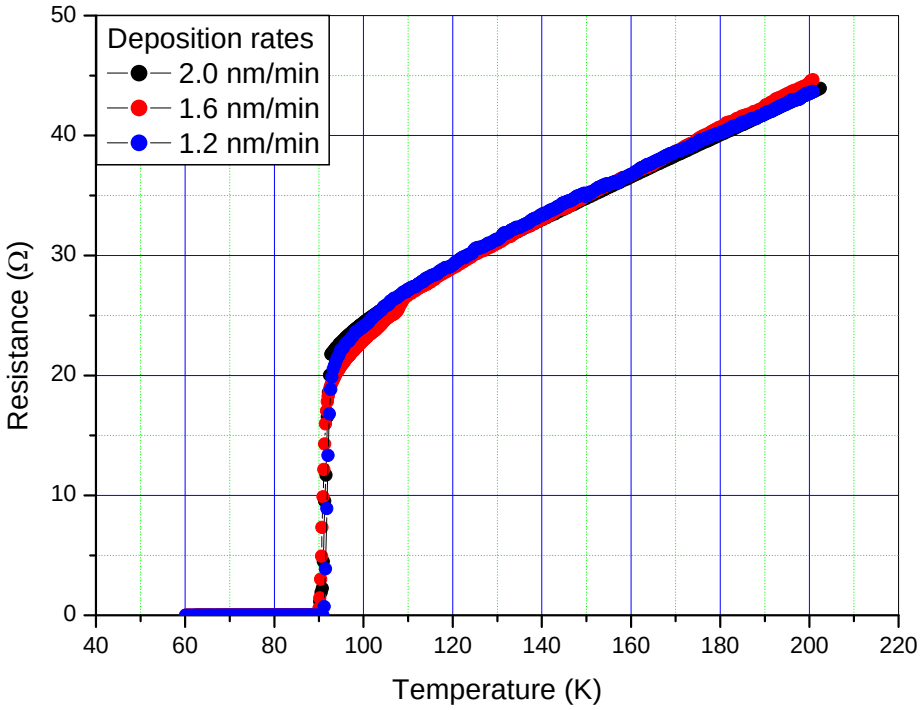

Figure 5.11. R-T curves of YBCO thin films deposited at different deposition rates relatively 1.2, 1.6 and 2.0 nm/min

Figure 5.11 shows the transition temperatures of the films deposited at different deposition rates. Thin films having 200 nm thickness were deposited onto 24-degree bicrystal $SrTiO_3$ (STO) substrates by varying the rate of film deposition between 1.2 nm/min and 2 nm/min. R(T) curves of these films are almost the same and the transition temperatures are showing slight variations between 89 and 91 K with transition widths of about 0.5 K.

a)

b)

c)

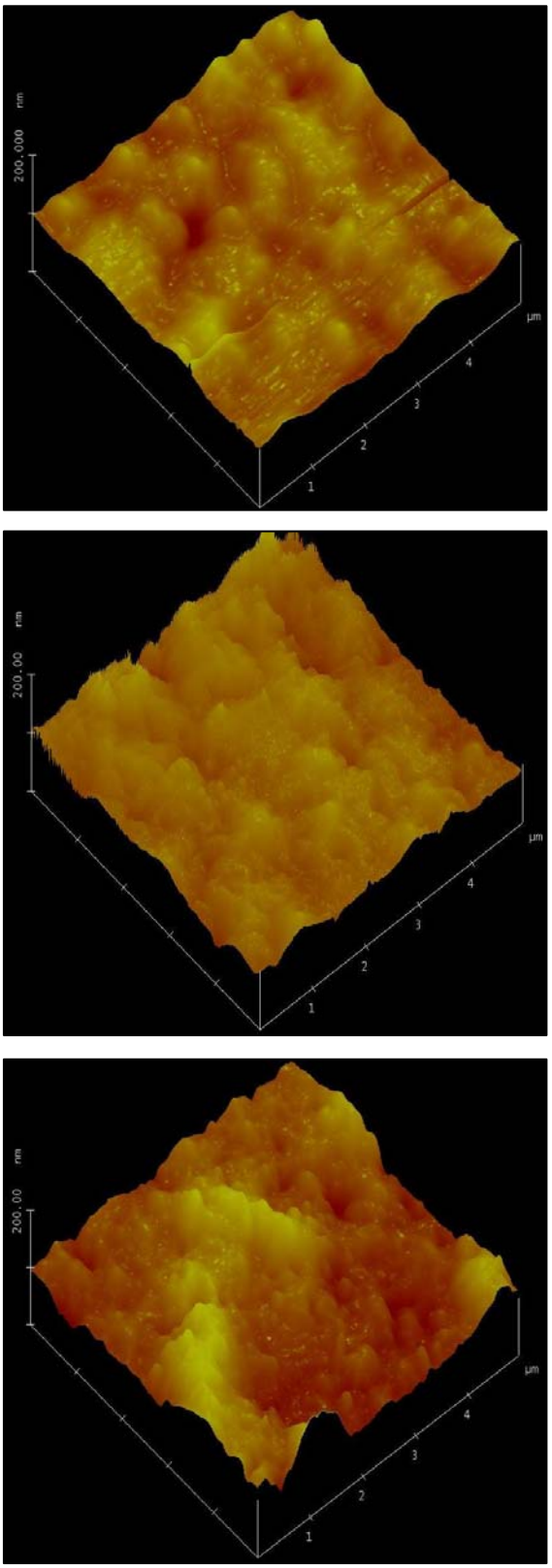

Figure 5.12. AFM images of YBCO thin films along the grain boundary region of bicrystal substrate depending on the film deposition rates of a) 1.2 nm/min, b) 1.6 nm/min, c) 2 nm/min

We obtained a relatively low value of 4 nm for the surface roughness of sample which was deposited at a rate of 1.2 nm/min and higher values for the samples with higher deposition rates

The samples were analyzed by XRD in order to obtain the effect of deposition rate on the YBCO thin film crystalline structure. As seen from Figure 5.13, the sample grown on (100) bicrystal STO substrate with a relatively low deposition rate of 1.2 nm/min shows a highly c-axis orientation. The peak intensities and the amount of c-axis orientation decrease as the deposition rate increases to 2 nm/min. Besides the c-axis orientation, we also observed a-axis orientation in sample 3 which was deposited at the rate of 2 nm/min. In this sample, in addition to the (003) and (006) c-axis peaks, (100) and (200) peaks of a-axis orientation appeared. The amount of c-axis orientations were determined from full width at half maximum (FWHM) values of rocking curves on the YBCO (005) peaks. The FWHM value of (005) peak of sample 1 deposited at a rate of 1.2 nm/min was determined to be 0.26^0 whereas that of samples 2 and 3, which were deposited with the rates of 1.6 and 2 nm/min were found to be 0.31^0 and 0.46^0 respectively.

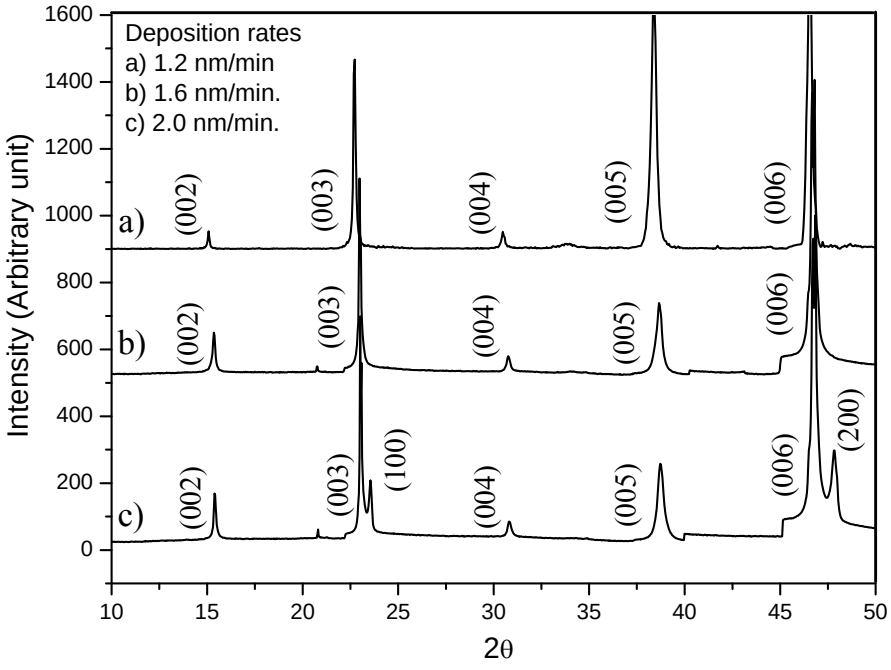

Figure 5.13. X-ray diffraction spectra of YBCO films grown at different deposition rates

The effect of $YBa_2Cu_3O_{7-\delta}$ (YBCO) thin film deposition rate on the I-V characteristics of bicrystal grain boundary Josephson junctions (GBJJs) were studied.In order to obtain different deposition rates between 1.0 and 2.0 nm/min for different samples (Liu, et al. 2001), we changed the plasma power from 40 to 80 Watts and adjusted the deposition time for obtaining the fixed film thickness of 200 nm. Superconducting transition temperatures of the samples were measured as 89-91 K. The deposition parameters, transition temperatures (T_c), FWHM values and surface roughness values (R_a) are given in Table 5.1.

Table. 5.1. The deposition parameters, transition temperatures, FWHM values and surface roughness of three different YBCO thin films with the same thickness of 200 nm.

Sample Number	Film Thickness (nm)	Deposition Rate (nm/min.)	T_c (K)	FWHM (degree)	Roughness (nm)
1	200	1.2	91	0.26	4
2	200	1.6	90	0.31	6
3	200	2.0	90	0.46	8

I-V characteristics of the JJs showed significant variation in the critical current and the normal state resistance values depending on the deposition rate as shown in Fig.5.14 and table 5.1. The I_c values decreased from 142 μA down to21 μA while the film deposition rate increased from 1.0 to 2.0 nm/min. one can say that the reason for these variations is that the film structure becomes non-homogeneous along the GB line as the deposition rate increases, resulting in the difference at JJs These non-homogeneous parts can consist of either non-superconducting or weakly superconducting zones depending on the oxygen content of the film in the GB, which may also be the reason for the increase in the normal state resistance of the junctions. The amount of non-superconducting or weakly superconducting parts can differ along the grain boundary, thus resulting in the variation of Josephson coupling between junctions. Another reason for this variation may be the occurrence of pin-holes or porous structures through the junctions during the high deposition rate. One can also

consider the partial decrease in the thickness of the film at the edges of the junctions as yet another reason because of higher surface roughness that comes with higher deposition rates.

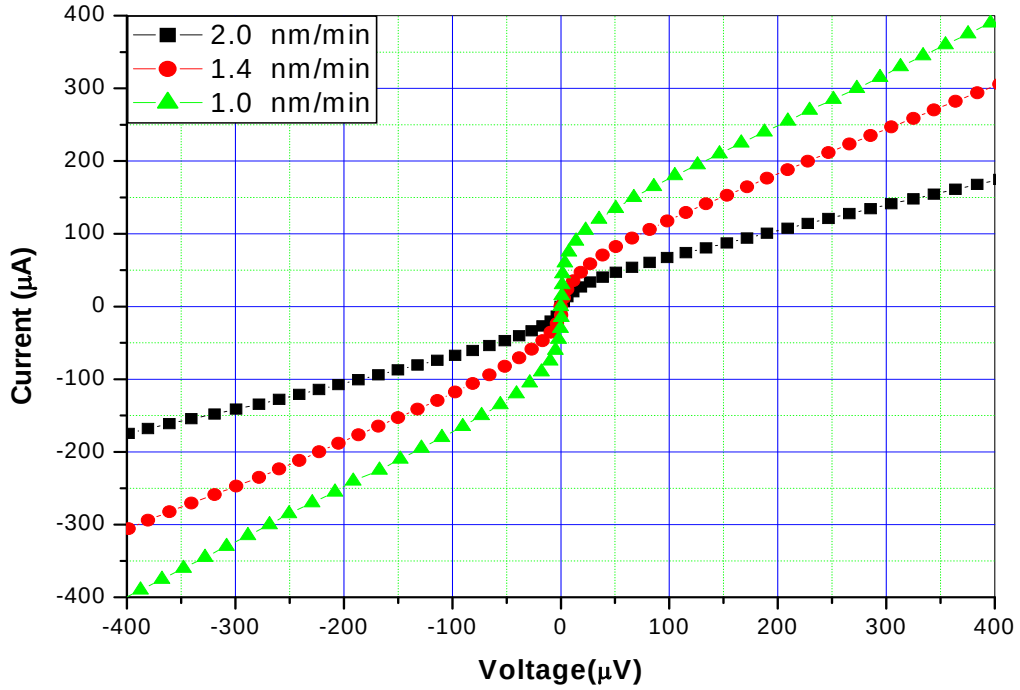

Figure 5.14. I-V characteristics of the GB Josephson junctions deposited at different rates.

The parameters obtained for the junctions including film deposition rate, critical current, normal resistance, I_cR_n product and surface roughness are given in Table 5.2.

Table 5.2. Properties of three different Josephson junctions as function of the YBCO thin film deposition rate

Sample Number	Film Thickness (nm)	Deposition Rate (nm/min.)	Junction Width (μm)	I_c (μA)	R_n (Ω)	I_cR_n (μV)
1	200	1.2	4	142	0.6	85
2	200	1.6	4	69	1.0	69
3	200	2.0	4	21	1.8	38

5.5.2. Effects of Thermal Cycles on I-V Characteristics of JJs

We investigated the effect of thermal cycling on the operation performance of (YBCO) JJs fabricated onto 24-degree SrTiO3 (STO) bicrystal substrates. Thin films having 200 nm thicknesses were deposited by dc-magnetron sputtering and device patterns were made by standard lithography process and chemical etching. The JJs having 4 μm widths were characterized by means of critical currents, In order to achieve a protective layer for the junctions against the undesired effects of thermal cycles and ambient atmosphere during the room temperature storage, the devices were coated with a 400 nm thick-YBCO layer at room temperature. Since the second layer of amorphous YBCO is completely electrically insulating, it does not affect the operations of the junctions. This two-layered configuration ensures the protection of the junctions from ambient atmosphere as well as from the effect of water molecules interacting with the film structure during each thermal cycle. The method in this study is based on the room temperature deposition of a 400 nm thick protective YBCO layer on top of the JJs. We used two different JJs; one without a protective layer and second with an amorphous YBCO protective layer. 200 nm–thick YBCO thin films were deposited by dc magnetron sputtering.

All of the measurements were made to investigate the effects of thermal cycling before and after passivation layer for two different JJs and results compare the devices characteristics depending on the cycling effects. The current-voltage characteristics of the devices were performed at 77 K under zero-applied field in magnetically shielded environment by directly dipping the JJs into liquid nitrogen. After finalizing the fabrication optimizations of the thin film deposition conditions and device fabrication process, I-V characteristics of JJs at the first thermal cycle showed that the properties obtained were close to the predicted values of the RSJ model having the critical currents of $I_c = 32$ μA and normal state resistance of $R_n = 2$ Ω with the product of $I_cR_n \approx 65$ μV. These values are typical for our JJs and small variations can be observed from device to device depending on the chemical etching process yielding the small difference in junction widths.

Current-voltage characteristics of the JJ without a protective layer showed significant differences after a number of thermal cycles regarding the degradation of critical current values as shown in Figure 5.15. We observed that both long term room

temperature storage and a number of thermal cycles between liquid nitrogen and room temperature are significantly affecting the junctions. For example, the critical current of the device at 77 K that we report in this study, reduced from 32 μA down to 2 μA and the normal state resistance, R_n, of the junctions increased up to 10 Ω at 77 K after approximately thirty cycles as shown in Figure 5.15.a.

Though we report the experimental results of a pair of JJs here, we observed that the uniformity and surface morphologies of the thin films deposited on top of grain boundary line of the substrates play important role on the thermal cycle dependence of the I-V characteristics of the devices as expected. We saw that the different substrates purchased from different manufacturers showed different thermal cycle stability. Although the devices without protecting layers showed different dependences against the number of cycles and storage time, all of them have tended to reduce the critical current values as well as the output voltage in long term usage. On the other hand, the JJs with 400 nm thick amorphous YBCO layer deposited on top of them have almost maintained the critical current values as well as the shape of I-V characteristics in that period of time including approximately thirty thermal cycles as seen in Figure 5. 15.

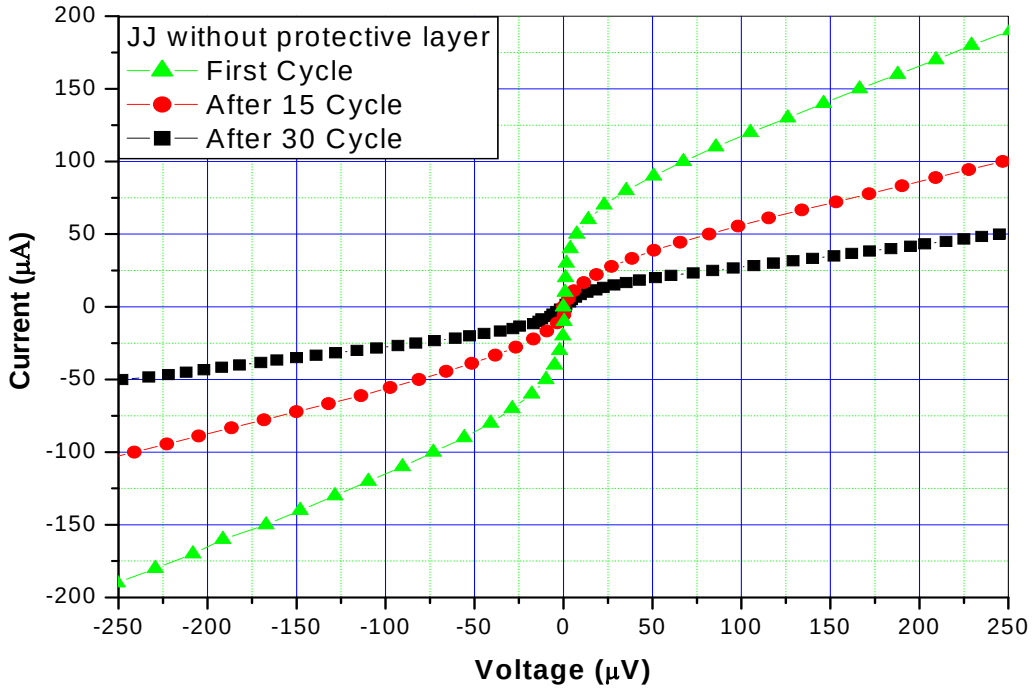

Figure 5.15.a. I-V characteristic of JJs at 77 K depending on the thermal cycles. Unprotected JJ, Solid, dotted and dashed lines represent the measurements for the first, 15th and 30th thermal

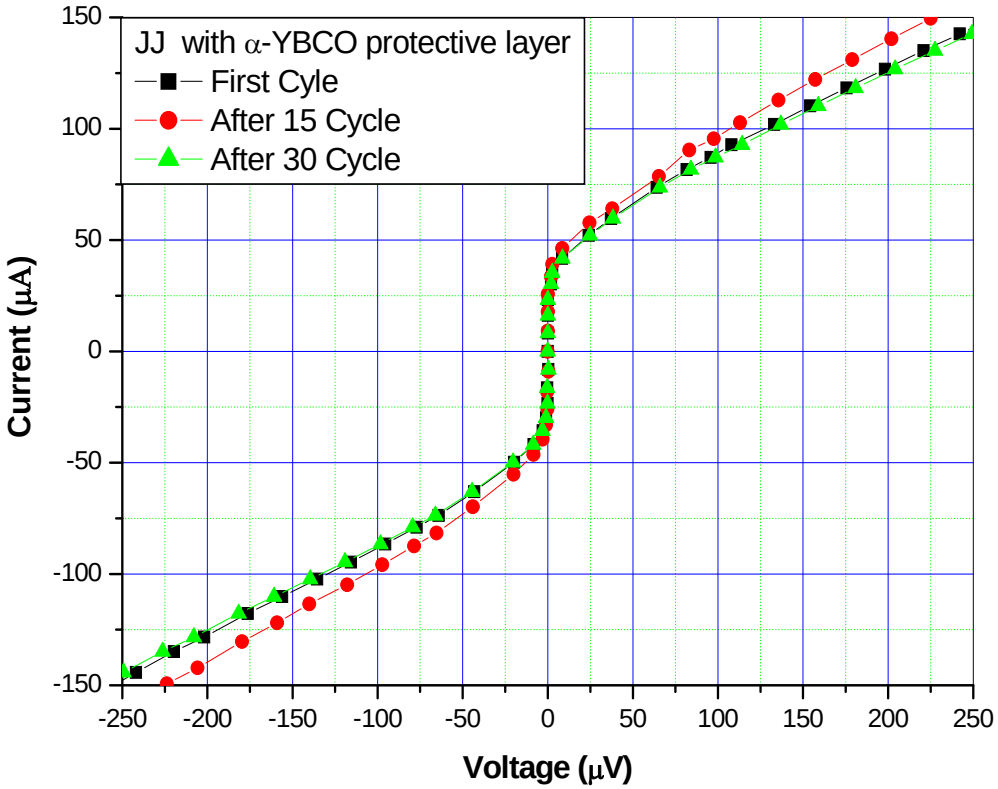

Figure 5.15.b. JJ with amorphous YBCO layer. Solid, dotted and dashed lines represent the measurements for the first, 15th and 30th thermal cycles respectively

CHAPTER 6

CONCLUSION

In this study, high-T_c YBCO Josephson junctions were fabricated and characterized. Fabrication steps of grain boundary Josephson junctions, including YBCO film deposition, patterning and etching processes have been introduced. Detailed explanation of the preparation steps of the samples after fabrication of YBCO thin films and characterization techniques used were presented in detail.

Structural characterization including AFM, SEM and XRD of the films on single and bicrystal substrates have been performed at IYTE Center for Material Research. For the photolithographic processes, the facilities at the Ege University Superconductivity Laboratory were used where the electrical characterization of the devices was also performed.

A measurement setup was designed for the electrical characterization of the devices, capable of conducting measurements such as current – voltage, resistance vs. temperature and magnetic susceptibility vs. temperature measurements. This setup was used to determine the electrical characteristics of the Josephson junctions.

AFM and SEM methods were utilized to investigate the structure of the deposited thin films. Crystallinity of the film was analyzed by XRD technique. Using these measurements, deposition parameters of the films were optimized in order to obtain consistent results regarding the critical currents and resistance of the junctions.

YBCO thin film deposition was performed using DC Inverted Cylindrical Magnetron Sputtering System (ICMS). Optimization of the thin film growth parameters was carried out entirely using single crystal substrates before the junction fabrication. After having a full control on the film properties, these deposition parameters have been used as a starting point for the optimization of the deposition parameters of YBCO thin films on bicrystal STO substrates in order to make Josephson junctions. To make junctions with junction widths between 2μm and 10μm, junction masks have been designed and fabricated using the facilities at TUBITAK-UEKAE.

Junctions have been fabricated on 24^0 and 30^0 bicrystal substrates after attempting to optimize the deposition parameters to produce high quality, stable and reproducible Josephson junctions. The optimization was carried out with respect to the

substrate orientation and junction width dependence. The deposition rate dependence of the junction critical current was investigated and a strong correlation between them was observed.

The effect of magnetic field on the current vs. voltage characteristics of the samples was examined by performing the I-V measurements under a magnetic field produced by a coil.

Thermal cycling effect on the current-voltage characteristics of Josephson junction was investigated. It was observed that it is possible to preserve the junctions against thermal cycles by covering the junctions with an amorphous YBCO layer.

REFERENCES

Anderson, P.W. and J.M. Rowell. 1963. Probable observation of the Josephson superconducting tunneling effect. *Physical Review Letters* 10(6):230-232.

Anderson, P.W. and A.H. Dayem. 1964. Radio frequency effects in superconducting thin film. *Physical Review Letters* 13:195-197.

Anocker, W. 1980. Josephson computer technology: An IBM research project. *IBM Journal of Research Development* 24(2):107-112.

Avci, I., M.Tepe and D. Abukay. 2004. Effect of deposition conditions on YBCO thin films by inverted cylindrical magnetron sputtering and substrate effects. *Solid State Communications and Technology* 130:357-361.

Avci, I., B.P. Algul and A. Bozbey. 2007. Investigation of the effect of thermal cycling on the device performance of YBCO DC-SQUIDs. *Superconductor Science and Technology* 20(10):944-9949.

Ayache, J. 2005. Grain boundaries in high temperature superconducting ceramics. *Phylosophical Magazine* 86(15):2193-2239.

Barone, Antonio and Gianfranco Paterno. 1982. *Physics and applications of the Josephson effect*. New York: John Wiley and Sons.

Beasley, M.R. 1999. High temperature superconducting thin films. *Proceedings of the IEEE* 77(8):1155-1163.

Beck, A.A. Stenzel and O.M. Froehlich 1995. Fabrication and superconducting transport properties of bicrystal Josephson junctions on different substrates. *IEEE Transactions on Applied Superconductivity* 5(2):2192-2195.

Bednorz, J.G. and K.A. Müller. 1986. Possible high-T_c superconductivity in Ba-La-Cu-O. *Physik B Condensed Matter* 64(2):189-193.

Beha, H. 1982. Mail: A new Josephson Family. *IEEE Journal of Solid-State Circuits*. 17(3):562-568.

Braginski, Alex, J. Krause and J. Vrba, eds. 2000. *Handbook of thin film devices.* New York: Academic.

Braginski, Alex I. 1993. *The new superconductcing electronics*. Dordrecht: NATO ASI series.

Chaudhari, P., J. Mannhart and D. Dimos. 1998. Direct measurement of superconducting properties of single grain boundaries in YBCO. *Physics Review Letters* 60:1653-1656.

Cogollo, R.P., A.C. Marino and H.M. Sanchez. 2003. Transport Properties of YBCO superconducting films at different oxygen concentration. *IEEE Transactions Applied Superconductivity* 13(2):2789-2791.

Delin, K.A. and A.W. Kleinsasser. 1995. Stationary properties of high-critical-temperature proximity effect Josephson junctions. *Superconductor Science and Technology* 9:227-269.

De Gennes, P.G. 1964. Boundary Effects in Superconductors. *Review Modern Physics* 36:225-237.

Dimos, D., P. Chaudhari and J. Mannhart. 1988 Orientation Dependence of Grain Boundary Critical Currents in YBa_2 Cu_3 O_{7-s} Bicrystals, *The American Physical Society,* 61(2):219-222.

Dimos, D., P. Chaudhari and J. Mannhart. 1990. Superconducting transport properties of grain boundaries in YBCO bicrystals. *Physical Review B* 41(7):4038-4049.

Feynman, Richard F., Robert B. Leighton and Matthew Sands, eds. 1965. *Feynman lectures on physics.* Burlington, MA: Addison-Wesley.

Gross, R., L. Alf and A. Beck. 1997. Physics and Technology of high temperature superconducting Josephson junctions. *IEEE Transactions of Applied Superconductivity* 7:2929-2935.

Gross, Rudolf and Achim Marx. 2005. *Applied Superconductivity: Josephson effect and superconducting electronics.* Garching, München University Press. http://www.wmi.badw.de/teaching/Lecturenotes/index.html (accessed October 30, 2006).

Golubov, A.A., M.Y. Kupriyanov and E. Il'ichev. 2004. The current phase relation in Josephson junctions. *Review of Modern Physics* 76:411-468.

Gonzales, J.K. 2005. Coated conductors and chemical solution growth of YBCO. *Universitat Autonoma de Barcelona Thesis of the Phd*.

Haage, T., J. Zegenhagen and J. Q. Li. 1997. Transport properties and flux pinning by self-organization in YBCO films on vicinal STO. *Physical Review B* 56(13):8404-8414.

Hadfield, R.H., 2002. Josephson junction fabricated by focused ion beam. *Trinity College-Cambridge University Thesis of the Phd.*

Hilgenkamp H. and Mannhart J. 2002. Grain Boundaries in high-T_c superconductors. *Review of Modern Physics* 74:485-549.

Jorgensen, J.D., M.A. Beno and D.G. Hinks. 1987. Oxygen ordering and the orthorhombic to tetragonal phase transition in YBCO. *Physical Review B* 36(7):3608-3616.

Josephson, B.D. 1962. Possible new effects in superconductive tunneling. *Physics Letter* 1: 251-253.

Kadin, Alan M. 1999. *Introduction to superconducting circuits.* New York: John Wiley and Sons.

Koelle, D., R. Kleiner and F. Ludwig. 1998. High-transition-temperature quantum interference devices. *Review Modern Physics* 71:631-686.

Koelle, D. 1999. High transition temperature superconducting quantum interference devices: basic concepts, fabrication and applications. *Journal of Electroceramics* 3(2):195-212.

Kunold, A., M. Hernandez and A. Myszkowski. 2007. *AC susceptibility in granular superconductors: Theory and experiment.* http://arxiv:cond-mat/0009429v1 (accessed September 27, 2005).

Lee, H.K., 2005. Growth, Microstructure and Ferroelectric Properties on Non-c-axis-oriented Rare-earth-substituted Bismuth Titanate Thin Films and Nanostructures. *Martin-Luther-University Thesis of the Phd.*

Likharev, K.K. 1979. Superconducting weak links. *Review Modern Physics* 51:101-159.

Likharev, Konstatin K. 1986. *Dynamics of Josephson junctions and circuits*. New York: Gordon and Breach Science Publishers.

Likharev K.K. and V.K. Semenov. 1991. RSFQ logic memory family: A new Josephson junction technology for subterahertz-clock-frequency digital systems. *IEEE Transaction on Applied Superconductivity* 1(1):3-28.

Lindström, T. 2005. d-wave Josephson junctions. *Chalmers University of Technology Thesis of the Phd.*

Liu, X.Z, Y.R. Li and B.W. Tao. 2001. The effect of deposition rate on the microstructure of YBCO thin films prepared by inverted cylindrical magnetron sputtering. *Physica C* 371:133-138.

McCumber, D.E. 1968. Effect of ac Impedance on dc voltage current charactereristics of superconductor weak-link junctions. *Journal of Applied Physics* 39(7):3113-3118.

Neils,W.K. 2002. Josephson interferometry measurements in high-T_c grain boundary junction. *University of Illinois Urbana-Champaign Thesis of the Phd*.

McBrian, P.F. 2000. Novel applications of the Josephson effect: Ferroelectric characterization and capacitively shunted boundary junction. *Pembroke College-Cambridge University Thesis of the Phd.*

Orlando, Terry P. and Kevin A. Delin, eds. 1991. *Foundations of Applied Superconductivity*. Prentice Hall.

Pagone, S. and A. Barone 1997. Josephson junctions. *Superconductor Science and Technology* 10:904-908.

Phillips, J. 1996. Substrate selection for high temperature superconducting thin films. *Journal of Applied Physics* 79:1829-1833.

Rowell, J.M. 1963. Magnetic field dependence of Josephson current. *Physical Review Letters* 11(5):200-202.

Rajiv, K.S., D. Kumar. 1998. Pulsed laser deposition and characterization of high-T_c YBCO superconducting thin films. *Material Science and Engineering* 22:113-185

Stewart, W.C. 1968. Current voltage characteristics of Josephson junctions. *Applied Physics Letters* 12:227-230.

Tafuri, F. and J.R. Kirthley. 2005. Weak links in high temperature superconductors. *Reports on Progress in Physics* 68:2573-2663.

Tahara S, S. Yorrozu and J. Komeda. 2001. Superconducting digital electronics. *IEEE Transactions on Applied Superconductivity* 11(1):463-468.

Tinkham, Michael. 1990. *Introduction to Superconductivity.* New York: McGraw Hill.

Weinstock, Harold, Richard W. Ralston, eds. 1993. *The new superconducting electronics*. London: Kluwer Academic Publishers.

Wördenweber, R. 1999. Growth of high-T_c thin films. *Superconductor Science and Technology* 12:86-102.

Wu, K.M., J.R. Ashburn and C. Torng. 1987. Superconductivity at 93 K in a new mixed-phase YBCO compound system at ambient pressure. *Physical Review Letters* 58(9):908-910.

Xing, W. B. Heinrich and J. Chrzanowski 1993. Determination of critical current densities of YBCO thin films AC susceptibility. *Physica C* 205:311-322.